Structure Determination of G Protein Coupled Receptor

by

Liang Jing

A Dissertation Presented in Partial Fulfillment
of the Requirements for the Degree
Doctor of Philosophy

Approved April 2022 by the
Graduate Supervisory Committee:

Yuval Mazor, Chair
Jeremy Mills
Xu Wang

ARIZONA STATE UNIVERSITY

May 2022

ABSTRACT

G protein coupled receptors (GPCRs) mediate various of physiological activities which makes them significant drug targets. Determination of atomic level structure of GPCRs facilitates the structure-based drug design. The most widely used method currently for solving GPCR structure is still protein crystallography especially lipidic cubic phase (LCP) crystallization. LCP could mimic the native environment of membrane protein which stable the membrane proteins. Traditional synchrotron source requires large size large size protein crystals (>30 micron) due to the radiation damage during data collection. However, acquiring large sized protein crystals is challenging and not guaranteed practically. In this study, a novel method was developed which combined LCP technology and micro-electron diffraction (MicroED) technology. LCP-MicroED technology was able to collect complete diffraction data sets from serval submicron protein crystals and deliver high resolution protein structures. This technology was first confirmed with soluble protein crystals, proteinase K and small molecule crystals, cholesterol. Furthermore, this novel method was applied to a human GPCR target, Î²2- adrenergic receptor (Î²2AR). The structure model was successfully built which proved the feasibility of applying LCP-MicroED method to GPCRs and other membrane proteins. Besides, in this research, a novel human GPCR target, human histamine 4 receptor(H4R) was studied. Different constructs were expressed, purified, and characterized. Some key residuals that affect ligand binding were confirmed.

DEDICATION

To mom and dad, who always give me unconditional love and support.

ACKNOWLEDGMENTS

I would express my appreciation to my advisor Dr. Wei Liu who currently works in University of Wisconsin Milwaukee. Thanks for all the guidance and advice. He worked so hard to apply funding to support my research and the whole group. I really appreciate the opportunity to work with you and other great lab members. I would like to thank Dr. Lan Zhu, thanks for teaching all the experimental skills and techniques. I would also like to thank to my other lab members Dr. Ming-Yue Lee Dr. Eugen Chun and Dr. Jinming Ma. I can't expect a better postdoc than you guys, I really appreciate all your help and mentorship for my projects. Dr. Zina AI-Sahouri and Dr. James Geiger, thanks for being a good colleague and I really enjoy the time working with you, I wish you have a wonderful career in the future.

Additionally, I would like to thank my collaborators. I would like to thank Dr. Brent Nannenga, thanks for your support with the MicroED project and Dr. Guanhong Bu, I really enjoy the time collecting diffraction data with you. Good luck with your research in UCLA.

Special thanks to Dr. Marcia Levitus and all my committee members Dr. Yuval Mazor, Dr. Jeremy Mills and Dr. Xu Wang. Thanks for your effort to help me finish the last step for my Phd career. It is really a hard time for me, and you really made my life easier. Thank you so much.

Finally, I would like to thank these important people in my whole life. My mom, Xinhong Li and dad, Xinsheng Jing. You are the best parents I can imagine. You work so hard and sacrifice so much to make me have a better life and achieve my dream. Shout out to all my best friends Jian Hu, Jin Li and everyone in the Dota2 group, thanks for all you company and all the happy nights we spent together on the

internet. Most importantly, I would like to thank my classmate, my girlfriend, my colleague, my life partner for now and the future, Dr. Chang Liu, you are the gift from God. Thanks for your company and support. It has been ten years since we met each other, and I can't wait to spend the rest of my life with you in Atlanta or anywhere in the world.

TABLE OF CONTENTS

Page

LIST OF TABLES

LIST OF FIGURES

CHAPTER 1
INTRODUCTION

1.1 G protein Coupled Receptors

G protein coupled receptors (GPCRs) are 7 helical transmembrane proteins which involved in a wide range of cell signaling pathways(Hilger, Masureel et al. 2018). The general structure of GPCRs consist of a N-termini region outside the cell membrane, 7 transmembrane helices and a C-termini region inside the membrane. Extracellular stimuli could trigger the intracellular physiological process through changing the conformation of related GPCRs. GPCRs then will induce the dissociation of G protein which will form a G alpha complex and a beta gamma complex that will further regulate the downstream signaling cascade.

Currently, there are over 800 known GPCRs which have a huge diversity in their primary protein structure, and phylogenetic classification utilized protein sequence as criteria to classify GPCRs into 5 subfamilies: Rhodopsin, Secretin, Adhesion, Glutamate, Frizzled/Taste2 (Hu, Mai et al. 2017). The Rhodopsin family is the largest family of GPCRs which contains about 701 human GPCRs (Figure 1.1). The N-termini of Rhodopsin family GPRCs is relatively short and has less diversity compare with other families (Soubias and Gawrisch 2012). However, the heterogeneity is huge no matter protein sequence or ligand binding preference, although they do have some highly conserved motifs within their transmembrane region. GPCRs represent critical drug targets because of the physiological functions they regulate(Congreve, Langmead et al. 2011). Knowing the structural details of membrane proteins will not only reveal the mechanism of the functions including

signal transduction, transportation and interaction between cells, but also facilitate the structure-based drug design(Congreve and Marshall 2010). Currently, X-ray crystallography is the most successful approach to obtain the high-resolution structure of membrane proteins(Shi 2014).

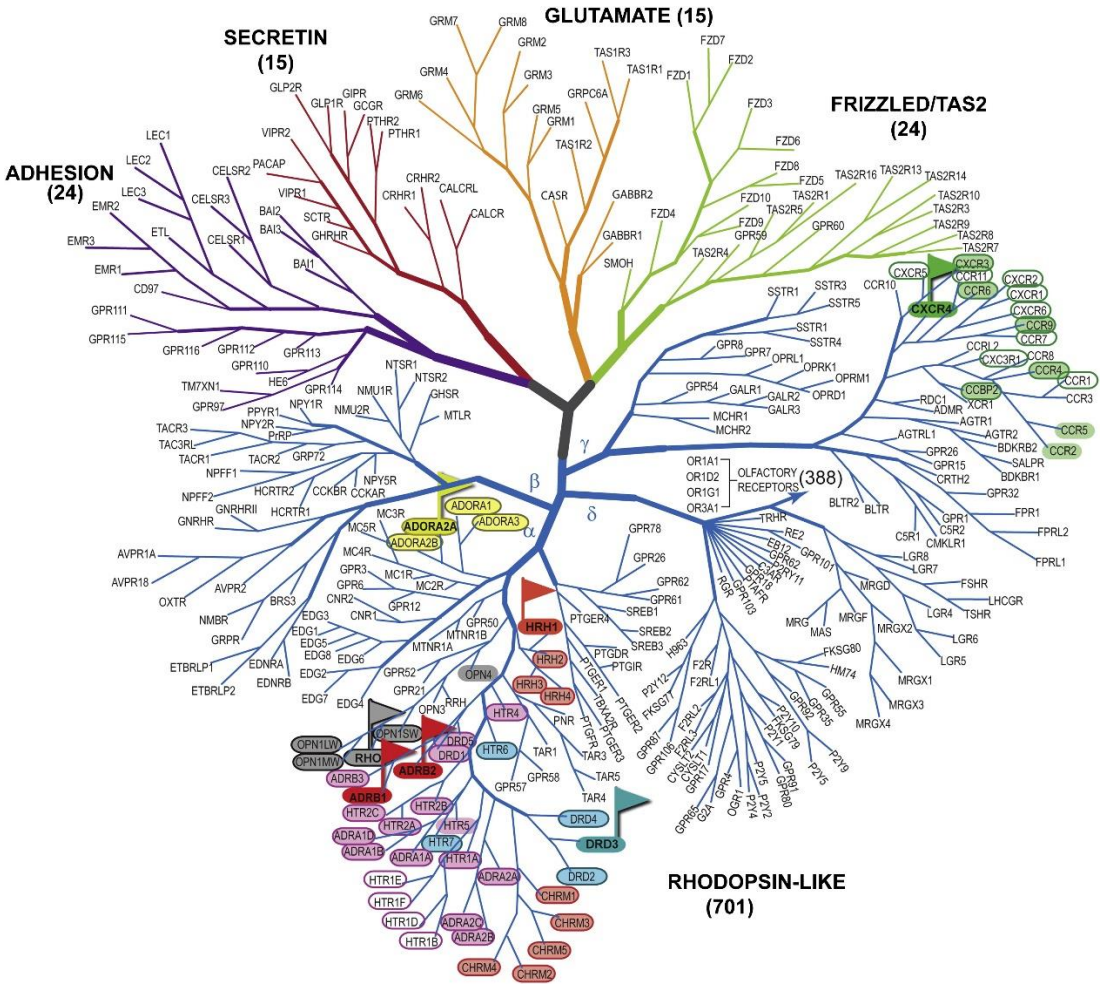

Figure 1.1 **GPCR Phylogenetic Tree Highlighting the Recently Solved GPCR Structures.**

Reprint with the permission from Kufareva, Irina, et al. "Status of GPCR modeling and docking as reflected by community-wide GPCR Dock 2010 assessment." Structure 19.8 (2011): 1108-1126.This is an open-access article distributed under the terms of the Creative Commons Attribution License (CC BY). The use, distribution or reproduction in other forums is permitted, provided the original author(s) or licensor are credited and that the original publication in this journal is cited, in accordance with accepted academic practice.

1.2 Membrane Protein Crystallization

Compared to soluble proteins, the native environment of membrane proteins is phospholipid bilayer which offers the membrane protein an intricate hydrophobic surrounding(Robertson 2018). Therefore, in the traditional crystallization trails, the first step of would be removing the membrane protein from the native cell membrane(Gruss, Hiller et al. 2015). Micelle method or so called in surfo method was introduced about 40 years ago which utilizes surfactants to generate micelles that incorporate membrane proteins and other impurities if present such as lipid residual and detergent(Michel, Huet et al. 1983). These membrane protein-embedded, water-soluble micelles are treated the same way as soluble protein in the crystal production process by vapor diffusion(Chayen 1998). This pure detergent-based method provides a hydrophobic condition that stabilizes the membrane protein, but the coverage of the membrane protein reduces the available surface area which is essential in protein crystal formation.

On the other hand, there is a pure lipidic method called lipidic cubic phase (LCP) or in meso method(Caffrey and Cheng 1995). LCP is an artificial membrane mimicking material that forms highly curved, continuously lipid bilayer. Briefly, the mechanism of LCP crystallization involves solubilizing the target membrane protein with specific detergent followed by purifying through various of chromatographic steps(Cherezov 2011). The purified target protein is then reconstituted in the LCP followed by a phase separation induced by precipitant solution which triggers the enrichment of target protein and facilitate the nucleation and crystal growth. Compared to the conventional crystallization method such as vapor diffusion, LCP

can increase the protein stability, has tighter crystal packing and has higher tolerance of impurity. The first successful application of LCP crystallization was the determination of bacteriorhodopsin(bR) at 2.5 angstrom resolution in 1996(Landau and Rosenbusch 1996). BR formed hexagonal plate shape crystals with dimensions of 20-40 μm × 20-40 μm × 5 μm within days. After this successful case, more and more membrane proteins, which could not be crystallized with vapor diffusion, have been successfully crystalized with LCP method(Shimamura, Shiroishi et al. 2011). Currently, according to the data from protein data bank (PDB), there are more than one thousand structures has been determined by LCP method and number of structures determined by LCP method is increasing every year.

Between the pure detergent-based method and pure lipidic based method, bicelles are two layers of micelles that formed by the mixtures of detergent and phospholipid(Poulos, Morgan et al. 2015). The disc like bicelles consist of two layers of phospholipid, whose polar head faces to the aquatic environment and the non-polar tail faces to the hydrophobic center of the bicelles. The edge of the bicelle is segmented and stabilized by the detergent molecule. The phospholipid can also provide a native like environment for the membrane protein and by various phospholipids can be used to modify the thickness of the membrane to accommodate different membranes. However, only few functional studies of membrane protein that employing bicelle method have been published so far(Faham and Bowie 2002). Nanodisc is a novel approach to solubilize the membrane which was first developed in 2007(Kijac, Li et al. 2007). Nanodiscs are nanoscale lipid bilayers that solubilize the membrane protein in a homological manner. The advantage of this method

includes homogeneity and long-term stability of the membrane protein. Like the bicelle method, nanodiscs also consist of phospholipid and detergent, what's more, they also need membrane scaffold protein (MSP) to control the dimeter of the nanodiscs(Bertram, Laursen et al. 2015). The ratio of all the constituents, include the target membrane protein, must be strictly controlled to form the proper nanodiscs. There are several MSPs available to be utilized to modify the size of the nanodiscs. The commonly used MSPs constructs are MSP1D1 which is used to form small nanodiscs with a dimeter of about 9.7 nm (Faas, Kiefer et al. 2018)and MSP1E3D1 that form larger nanodiscs with a dimeter of about 12.9 nm. There are also MSPs that can result in even larger nanodiscs.

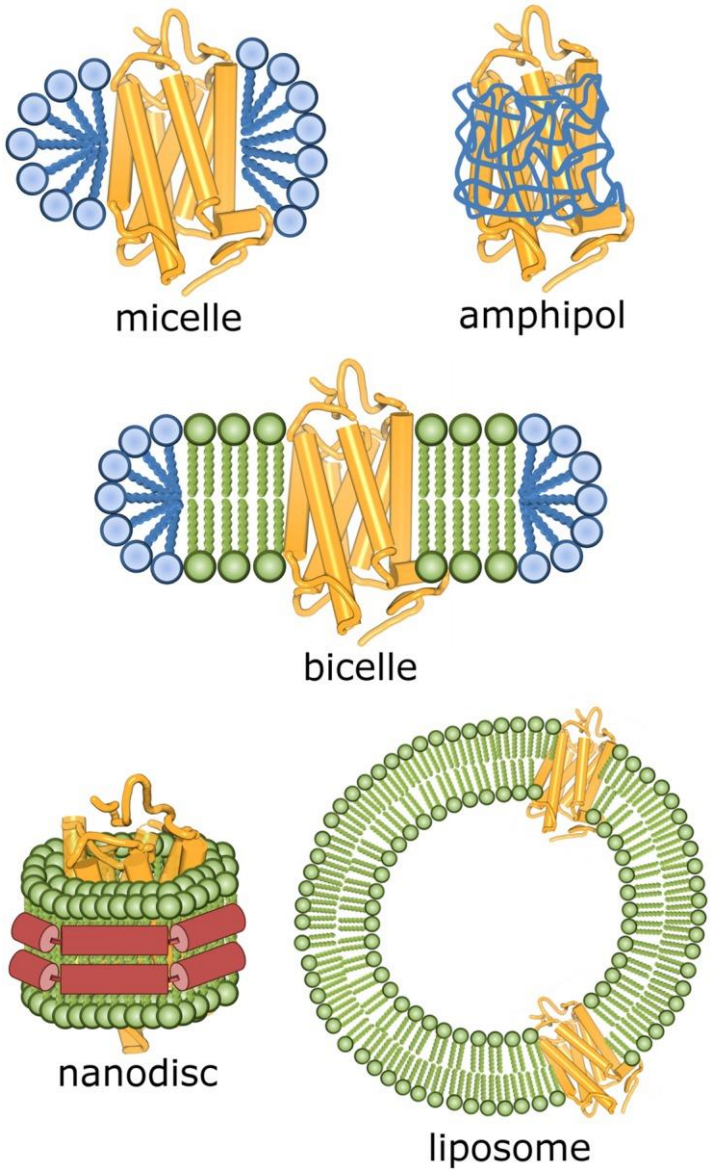

Figure 1.2 **Schematic Representation of Some Possible Environments for GPCR.**

Reprint with the permission from Milić, D., & Veprintsev, D. B. (2015). Large-scale production and protein engineering of G protein-coupled receptors for structural studies. Frontiers in pharmacology, 6, 66. This is an open-access article distributed under the terms of the Creative Commons Attribution License (CC BY). The use, distribution or reproduction in other forums is permitted, provided the original author(s) or licensor are credited and that the original publication in this journal is cited, in accordance with accepted academic practice.

1.3 LCP Crystallization

The mesophase or so called liquid crystalline state is an intermediate state between solid and liquid. And the lipid constitutes cell membrane where the membrane proteins reside has a capacity to form mesophase. The formation of mesophase is in a spontaneous manner, in another word, no external energy such as ATP is required during the formation of mesophase(Briggs and Caffrey 1994). Mesophase is a result of amphiphilic interaction among the lipid molecule who has both polar and non-polar parts. When the aquatic component induces the phase separation as described before, hydrophobic effect plays a crucial role.

The mesophase (Figure 1.3) is a combination of serval states which can be classified into two categories: 1) lamellar liquid phase(L_α) 2) non-lamerllar phase. This includes the inverted hexagonal phase (H_{II}) and cubic phases (Pn3m, Ia3d and Im3m). The specific phase is affected by several factors that includes temperature, pressure, lipid type and concentration and the aqueous dispersing medium(Chung and Caffrey 1994).

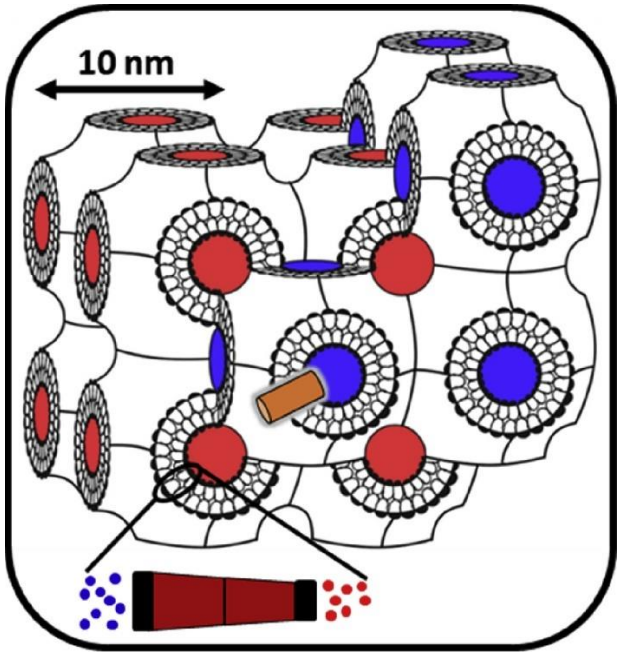

Figure 1.3 A Schematized View of the Bicontinuous Lipid Cubic Mesophase

Reprint with the permission from Li, D., & Caffrey, M. (2020). Structure and functional characterization of membrane integral proteins in the lipid cubic phase. Journal of Molecular Biology, 432(18), 5104-5123. This is an open-access article distributed under the terms of the Creative Commons Attribution License (CC BY). The use, distribution or reproduction in other forums is permitted, provided the original author(s) or licensor are credited and that the original publication in this journal is cited, in accordance with accepted academic practice.

The in meso crystallization process is different with traditional sitting drop or hanging drop crystallization(Li, Howe et al. 2014). The purified protein solution needs to mix with the host lipid and form transparent LCP, then about 40 nL protein-laden LCP is dispensed on a glass plate followed by jetting about 800 nL precipitant solution on the LCP drop. Finally, another glass cover slip is covered. The precipitant solution will diffuse towards the center of LCP through the water channel of LCP, the diffusion of precipitant solution breaks the balance of the initial LCP environment and induces the phase changes, from LCP to lamellar phase. If under the ideal situation, the phase flipping may induce the nucleation of the

protein and the protein molecule from the neighboring region will keep diffusing to this crystal nuclear through the capillary-like lamellar phase(Figure 1.4). This is the most acknowledged hypnosis describing the crystallization mechanism of in meso crystallization and the fact that all the protein crystals that crystalized in LCP are in type I packing proves this hypothesis indirectly(Cherezov 2011).

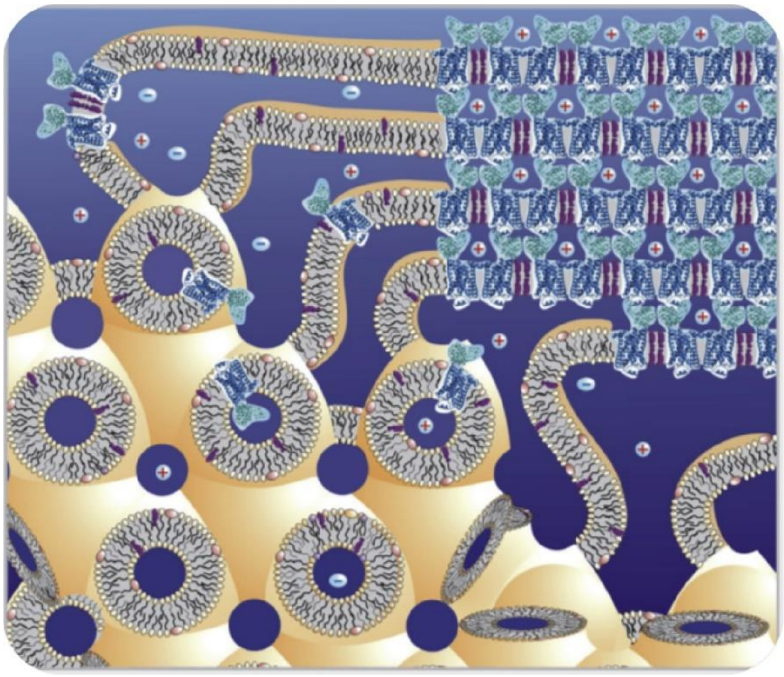

Figure 1.4 Events Proposed to Take Place During the Crystallization.

Reprint with the permission from Li, D., & Caffrey, M. (2020). Structure and functional characterization of membrane integral proteins in the lipid cubic phase. Journal of Molecular Biology, 432(18), 5104-5123. This is an open-access article distributed under the terms of the Creative Commons Attribution License (CC BY). The use, distribution or reproduction in other forums is permitted, provided the original author(s) or licensor are credited and that the original publication in this journal is cited, in accordance with accepted academic practice.

1.4 Advantages of LCP crystallization

1.4.1 Minimize the consumption of protein

In the protein crystallization field, the yield of the target protein is always a challenge especially for the membrane proteins expressed in eukaryotic cell lines. Even the target protein is expressed in the bacterial expression system and has a relatively high expression level, the amount of pure, homological, and stable target protein might be rare after the purification steps. Compare with the traditional crystallization method, vapor diffusion or batch method, which require ~100 nL protein for each condition, the LCP crystallization reduce the protein consumption to 40 nL each condition(Liu and Cherezov 2011). Using LCP crystallization method, 2.5 times more condition can be tested with the same amount of precious protein sample, which save labor and budget dramatically.

1.4.2 Produce high quality crystals

In the LCP crystallization method, the target protein is reconstituted in a cubic phase bilayer. Both aqueous channel and lipidic bilayer are continuous in 3D space. According to the mechanism of the protein crystal formation in LCP, the precipitant solution will induce the phase separation of the local LCP and initiate nucleation which in further create a portal for the protein to diffuse from the cubic phase reservoir to the crystal nuclear. If the protein indeed crystalizes in this manner, type I crystal will be formed. Furthermore, LCP can provide the convection-free environment for protein to crystalize which is similar with the microgravity

crystallization. This condition provides a stable zone for the crystal to pack in a slow and order manner. What's more, it avoids the impurities to cover on the surface of the crystal to block the growth of the crystal.

Accordingly, in meso method crystallization usually generates small crystals which benefits the diffraction data collection in the microbeam. Because the beam size matches the size of the crystal, the background scattering, and the diffraction from the mesophase are reduced. This advantage was used in the bR work and other GPCRs structure determination(Panneels, Wu et al. 2015).

1.4.3 Available for Rational Design for Optimization

The crystallization optimization process of in surfo crystallization method usually focus on the protein quality and precipitant solution. As for LCP crystallization method, beside of improving the protein quality and testing various of precipitant solution, a few parameters are available for optimization which provide more possibility of the protein to crystallize.

The most used lipid in LCP crystallization is monoolein (1-Oleoyl-rac-glycerol), however, the protein may have difference in the ordinate axis, the requirement of the thickness may be different as well. The optimization of the host lipid may potentially solve this problem.

Some small molecules play critical role in the stabilization of the target protein,

however, due to the poor solubility, these small molecules cannot be added into the protein solution. LCP crystallization method offers a path to supplement these hydrophobic molecules with the protein by dissolving the small molecule into the host lipid.

1.4.4 Pre-crystallization Screening

Protein crystallization usually require relatively high concentration of target proteins. As mentioned before, the acquisition of target protein is sophisticated. In surfo crystallization method, in some ways, is a "yes or no" gamble. No useful information could be obtained from a failed crystallization attempt. In another words, precious protein sample is wasted for nothing valuable except for "This batch of protein is not good enough" or "This precipitant solution doesn't work". However, the in meso method create a possibility to perform pre-crystallization screen which consume small amount of protein and provide valuable information about protein quality and diffusion rate of the protein in the LCP matrix in a high-throughput manner. LCP-Tm and LCP-FRAP are the commonly used method to collect this information.

LCP-Tm, first introduced in 2010, is a robust and accurate assay to evaluate the thermal stability of membrane proteins in LCP(Liu, Hanson et al. 2010). With temperature ramping, membrane protein embedded in LCP will be denatured, so that the fluorescence change resulting from either ligand release or cysteines binding with a thiol-binding reporter dye exposure, can be quantified. The thermostability of the target protein can be evaluated. LCP-Tm assay is commonly used to screen the ligand

of the target. Moreover, potential host lipid and lipid additives that can further increase the protein stability can be optimized.

Fluorescence recovery after photobleaching (FRAP) was developed in 1976 and was used to study the diffusion rate of membrane protein in LCP in 2008(Cherezov, Liu et al. 2008). It was found that both protein construct and crystallization conditions are associated with the diffusion properties of membrane proteins in the LCP matrix. Common precipitants often induce unwanted aggregation of membrane proteins, preventing crystal nucleation in LCP. There is a very high correlation between the diffusion rate and crystallization conditions. Thus, in LCP-FRAP, crystallization conditions as well as suitable constructs, stabilizing ligand, that are beneficial to diffusion, nucleation and crystal growth can be selected out only with micrograms of protein sample. With the development of instrument and software, this assay could be performed in a high-throughput manner. It only takes ~30 mins to get the readout of a 96-well plate. The software can evaluate the result automatically, in some cases, initial hits may be found in the high score wells. Even without any hits in the whole plates, the high score wells are good points of penetration. In the worst case, all wells give low scores, which indicate this protein can barely diffuse in the meso phase, in another words, it has very low possibility to crystallize. Even the worst situation can provide useful information and save time and effort.

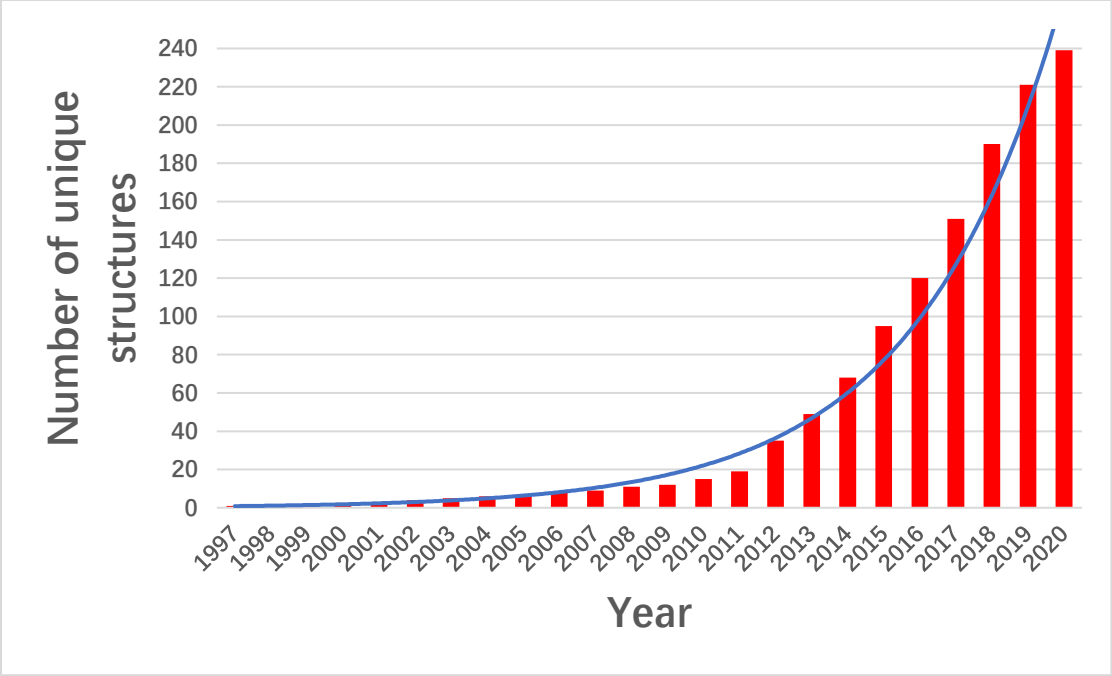

Figure 1.5 **Structure Determination by LCP Crystallization**. As of this writing, there are close to 10,000 structures deposited in protein data bank (PDB) attribute to the LCP or in meso method and about 200 structures of them are membrane protein.

1.5 Micro-Electron Diffraction (MicroED)

Synchrotron was widely used in the original LCP crystallization due to its redundancy and accessibility. However, the data collection process at synchrotron facility has limitation. Frist of all, the data collection at synchrotron source requires large protein crystals which are not easy to obtain. To acquire large size protein crystal, couple rounds of optimization are necessary. The crystallization optimization may take months to years and the large crystals are not guaranteed. Secondly, the protein crystals in LCP crystallization must be handled by skilled personal, especially the crystal harvesting process. The LCP drop which contain the

protein crystals is in the middle of the glass sandwich plate, the glass cover slip must be broken without mixing too much broken bits of glass into the LCP drop. Besides, LCP is a toothpaste-like matrix, because of the high viscosity of LCP, fishing the protein crystal with the metal loop is not as easy as harvesting crystals from a sitting drop plate. What's more, the data collection at synchrotron source requires a continuous exposure of the protein crystal which may lead to severe radiation damage to the protein crystal. With the development of the innovative technology, especially the brilliant beam source and the sample deliver methods, these problems have been solved at certain degree.

Micro-electron diffraction is a cryo-electron microscopy-based technology that employs electron beam to determine high resolution structure form nano-sized protein crystals which are only couple protein layers thick(Mu, Gillman et al. 2021). Nano-sized protein crystals are loaded on the regular EM girds followed by bolting. Then the grids are vitrified by liquid ethane and kept in the cryogenic environment to maintain the hydration of the sample in the vacuum condition and reduce the radiation damage(Bu and Nannenga 2021). Similar with the traditional data collection at synchrotron source, multiple diffraction pattern can be recorded from one single crystal by tilting the sample stage, which reduce the sample consumption when comparing with the serial crystallography methods(Ohmer, Dasgupta et al. 2022). Moreover, the diffraction data can be processed with the common crystallographic data processing software without knowing the unit cell parameter in advance. The advantage of micro-ED includes 1) The electron beam has much stronger interaction with matter and less radiation damage compare with the X-ray.2) The cost of building a synchrotron or

XFEL facility usually is over billion dollars, whereas the cost of a cryo-electron microscopy is in the range of million dollars. And the maintenance of a cryo-electron microscopy is more budget friendly. 3) The sample consumption of micro-ED is less than SX and the facility has better accessibility.

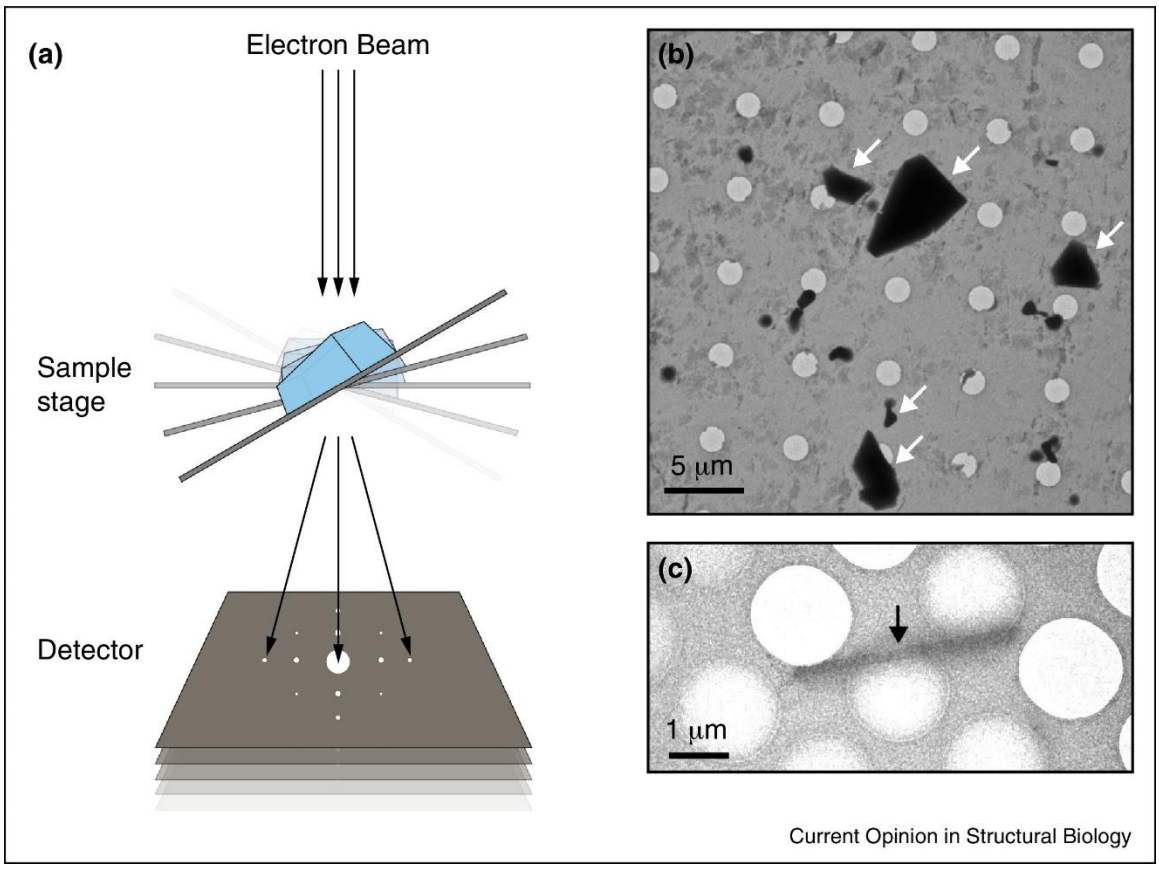

Figure 1.6 **MicroED Data Collection and Microcrystal Visualization**. (A) Schematic of MicroED data collection by tilting the sample stage between subsequent exposures. Each exposure is of relatively low dose (~0.01 $e^{-}/Å^{2}/s$) which allows the collection of multiple diffraction patterns from a single crystal that are combined into a single data set. Each data set consists of up to 90 still frames taken at 0.1°–1° intervals. (B, C) Visualizing microcrystals (arrows) in the TEM prior to data collection. The dimensions of microcrystals suitable for MicroED range from approximately 1–10 μm

in length and width and 0.1–1 μm in thickness. The crystals of a membrane transporter (B) visualized by negative stain EM, whereas the crystals of a novel designed protein (C) are seen with cryo-EM in over-focused diffraction mode.

Micro-ED has been used to determine many high-resolution protein structures and small molecule structures(Nannenga, Shi et al. 2014, Vergara, Lukes et al. 2017). However, most of them are soluble protein.

1.6 LCP-MicroED

Few membrane protein structure has been determined by micro-ED method due to the intrinsic straits of membrane crystallography and other challenges of sample preparation such as applying the membrane protein crystals on the grids without reducing the crystal quality dramatically. Thus, the combination of LCP and micro-ED may create a new path of the membrane protein structure determination. So far, this area is still in the prove of concept stage. Initially, proteinase K, a model of soluble protein, was crystalized using batch method, and reconstituted in LCP. However, LCP is too viscous to be deposited directly on the grids, additive need to be mixed with the crystals-laden LCP to convert LCP to sponge phase which is less viscous and make it possible to load the crystal sample on the grids. The structure of proteinase K was

solved successfully with 2.0 Å resolution(Zhu, Bu et al. 2020). One of the actual membrane proteins, human adenosine A2A receptor ($A_{2A}AR$) which was crystalized in LCP, was tested with micro-ED as well and diffraction patterns were obtained but more diffraction patterns were needed to determine the structure. Objectively, LCP-MicroED is a novel technology of structure determination and it still need a lot of effort from the pioneers to optimize the protocol and determine more structures especially membrane protein structures to prove the concept. In the future, LCP-MicroED may become a supplementation for X-ray crystallography.

CHAPTER 2

STRUCTURE DETERMINATION OF HUMAN HISTAMINE 4 RECEPTOR

2.1 Abstract

G protein-coupled receptors (GPCRs) are 7 helical transmembrane proteins which play a crucial role in cell signaling pathways through their interaction with G protein. This project is focused on a histamine family receptor which is involved in the human inflammatory responses and allergy. And the disorder of histamine receptor could lead to several diseases. The structure determination of histamine could accelerate the development of new drugs that target on histamine receptor. The preliminary goal of this project is optimizing a construct which could be expressed in sf9 cell line and generate target protein with high yield, thermostability and homogeneity. Different protein engineering strategies such as fusion protein insertion at inter cellular loop (ICLIII), N termini and C termini truncation and site mutations were applied during construct optimization. The yield and quality of target protein were successfully improved comparing with the wild type. And the optimized construct was used to screen the ligand which could significantly increase the protein homogeneity and thermostability. Future work includes further optimization of the N-termini fusion and mutations. LCP-FRAP (Lipidic Cubic Phase-Fluorescence Recovery After Photobleaching) would be applied when better constructs were obtained. Co-expressing with G protein or forming GPCR G protein complex in vitro and determine the structure through cryo-EM could be another option.

2.2 Introduction

In recent years, more than 30 high resolution GPCR structures have been solved due to the innovative protein engineering strategies and successful application of Lipidic cubic phase (LCP) in protein crystallization(Xiang, Chun et al. 2016). High resolution GPCR structures have not only helped elucidating the mechanism of GPCR activation, inactivation, and allosteric modification, but also accelerated the discovery of new drugs targeted on GPCRs(Congreve and Marshall 2010). For example, how sodium ions regulate the receptor and how cholesterol stabilize the receptor was illuminated based on the 1.8 Å structure of a A_{2a} adenosine receptor(Liu, Chun et al. 2012). The recent success in GPCR crystallization relies on the application of LCP technology. LCP is a phase that obtained through mixing aqueous and lipid in a specific ratio based on the type of lipid. LCP is believed to facilitate the crystal packing by providing an environment which is similar with the cell membrane. In 1996, LCP technology was first applied to solve the structure of bacterial rhodopsin(Pebay-Peyroula, Rummel et al. 1997), and the first human GPCR structure, ß2 adrenergic receptor, was solved in 2007 and LCP was also used in the crystallization(Cherezov, Rosenbaum et al. 2007). Besides, new LCP technologies have been developed to increase the efficiency of crystallization such as LCP-FRAP. This assay could measure the diffusion rate of membrane proteins in LCP matrix which is crucial for protein crystallization. Too high or low diffusion rate will lead to the failure of crystal packing. And this assay has allowed crystallographers to better screen the crystallization conditions.

Histamine receptor family belongs to the rhodopsin family(Thangam, Jemima et al. 2018). Histamine is the natural agonist for this family which mediates the pathways for allergic response and asthma. There are four known subtypes in this family and based on the time of discovery, they were named Histamine 1 receptor(H1R), Histamine 2 receptor(H2R), Histamine 3 receptor(H3R) and Histamine 4 receptor(H4R). Only one structure of H1R bound to the first-generation H1R antagonist doxepin was solved so far(Shimamura, Shiroishi et al. 2011). It's worth noting that doxepin could also bind with H2R and H4R which makes the first-generation drug that targets H1R has been shown to have side effects. Thus, the determination of more structures of histamine receptor family will attribute to the discovery of new drug which has less side effects and non-specific binding.

One of the main reasons that makes GPCR crystallization challenging is the flexibility of the structure ,especially N-termini and ICLⅢ, and lack of polar surface area. Besides, the relatively low expression level and lack of stability could also make GPCR crystallization difficult. The successful protein engineering strategies have been applied in GPCR crystallization include fusion proteins, truncations, and Mutagenesis.

N-termini and ICLⅢ are the most flexible regions of one GPCR because they usually don't have a stable secondary structure such as alpha-helix and beta-sheet(Katritch, Cherezov et al. 2013). Although directly truncation of N-termini and ICLⅢ could increase the stability, it could also reduce the polar surface area which will make GPCRs hard to crystalize. Therefore, fusion proteins have been screened to replace these regions. Theoretically, the replacement of ICL Ⅲ with fusion protein could not

only increase the stability of GPCRs, but also maintain or increase the polarize surface area. The ideal fusion proteins are stable, compact, and easily to be crystalized. Nowadays, the most widely used fusion proteins is T4 lysozyme(T4L), about half of the existing GPCR structures have been solved with T4L as a fusion domain no matter at ICL Ⅲ or N-termini. The second most popular fusion protein is a thermostabilized apocytochrome b_{562}RIL(Bril), a few other fusion proteins have also been used in CPCRs crystallization such as Rubredoxin and *Pyrococcus abyssi* glycogen synthase (PGS). However, the insertion position of the fusion protein could have unpredictable effects on protein expression, protein stability or both, so the best insertion position needs to be experimentally determined(Xiang, Chun et al. 2016).

The N, C-termini truncation could also be an option to stabilize the protein, however, the N, C-termini truncation has more significant effects of the expression level even the relationship is unpredictable. In general, the length of N or C termini in most of the crystallized GPCRs is less than 40 amino acid residues and this observation matches the fact that GPCRs with longer termini are more difficult to crystallize.

Mutagenesis has also been a choice to expedite GPCRs crystallization. Predominantly, the purposes of mutating specific amino acids in GPCRs are: (1) removing the post-translational modifications (PTMs) which usually are glycosylation. (2) increasing the expression level of GPCRs. (Chen, Arendall et al.) increasing the thermostability of GPCRs.

2.3 Method

2.3.1 Expression and Purification of H4R

The cDNA of histamine receptor was obtained from DNASU and cloned on pFastBac plasmids (Invitrogen). All the constructs generated in this project have uniform elements: a poly H promoter, N-termini HA tag followed by a FLAG tag. Histamine 4 receptor gene is in the middle and there is a PreScission protease site followed by a 10X His tag in the C-termini. Asc Ⅰ and Hind Ⅲ restriction enzyme cutting sites were located at the beginning and end of the histamine receptor gene respectively. The Bac-to-Bac Baculovirus Expression System (Invitrogen) was used to express the histamine receptor, and both the total and surface expression data was measured and analyzed by a flow cytometer (EMD Millipore).

The harvested cells were lysed and washed in both low salt lysis buffer (10 mM HEPES pH 7.5, 10 mM MgCl2, 20 mM KCl) and high salt lysis buffer (10 mM HEPES pH 7.5, 10 mM MgCl2, 20 mM KCl, 1M NaCl) respectively, then the washed pellet was resuspended in resuspension buffer (10 mM HEPES pH 7.5, 10 mM MgCl2, and 20 mM KCl, 30% glycerol, protease inhibitor). 2 mg/mL iodoacetamide(Sigma-Aldrich) was added in the pre-solubilization step, after 30 min incubation at 4 ℃, solubilization buffer (50 mM HEPES pH 7.5, 1M NaCl, 1%/0.2% DDM/CHS) was add and then incubate for 2.5 hours at 4 ℃ while shaking. The material that cannot be solubilized was removed by centrifugation and the supernatant was incubated with 2.5% (V/V) TALON IMAC resin(Takara Bio) and 10 mM imidazole overnight at 4 ℃.

The resin was washed with twenty column volume of wash buffer 1 (25 mM HEPES pH 7.5, 800 mM NaCl, 0.1%/0.02% DDM/CHS, 20 mM imidazole) and followed by 10 column volume wash of wash buffer 2 (25 mM HEPES pH 7.5, 500 mM NaCl, 0.05%/0.01% DDM/CHS, 20 mM imidazole). Finally, the protein was eluted using 5 column volume of elution buffer (25 mM HEPES pH 7.5, 500 mM NaCl, 0.05%/0.01% DDM/CHS, 200 mM imidazole). SDS-PAGE and size exclusion chromatography were performed to analyze the purity and homogeneity of histamine receptor.

2.3.2 Thermostability Assay

N-[4-(7-diethylamino-4-methyl-3-coumarinyl) phenyl] maleimide (CPM) dye (Invitrogen) was dissolve in DMSO at 4 mg/mL as stock solution and stored in -80 ℃ for future use. Desalt buffer (25 mM HEPES pH 7.5, 500 mM NaCl, 0.05%/0.01% DDM/CHS) was used to dilute the CPM dye stock at 1:40 ratio. Histamine receptor was concentrated using a 100 kD concentrator (EMD Millipore), and about 4 μg protein was then diluted with desalt buffer to the final volume 130 μL. 5μL diluted CPM dye was added to the solution and incubate for 30 min on ice in the dark environment. All mixed solution was then move to a quartz fluorometer cuvette (Stama Cells) and the data was collected by Cary Eclipse spectrofluorometer (Varian). The temperature range of this assay was from 20 ℃ to 95 ℃ with a temperature ramping rate at 1 ℃ per minute. Collecting data was processed with GraphPad Prism (Graphpad Software) and a Bolzmann sigmoidal equation was used to fit the curve and determine the melting temperature.

2.3.3 Expression of G Protein and scFv16

The expression of G protein complex was followed the protocol that published previously(Dror, Mildorf et al. 2015). Briefly, G protein alpha subunit was expressed by *Escherichia coli* (BL21). The biomass was resuspended with low salt buffer and treated with sonicator. The supernatant was mixed with Ni-NTA resin. After 2 hours binding, the resin was washed with wash buffer and the protein was eluted with elution buffer which has 200 mM imidazole. G protein beta and gamma subunits and scfv16 protein were expressed by insect cell expression system (sf9)(Koehl, Hu et al. 2018). For G protein beta and gamma subunits expression, the gene of these two proteins were cloned into pFastbac Dual vector which has two promoters that enabled these two proteins to be expressed simultaneously. The following expression and purification steps were the same with H4R expression. The expression of scfv16 is same with H4R expression as well, however, a GP67 signaling peptide was inserted at the N-termini of scfv16 which make scfv16 to be secreted. When collected the biomass, the cell pellet was discarded, and the supernatant was collected. The supernatant was then mixed with Ni-]NTA and purified the eluted with gravity column and fast protein liquid chromatography(FPLC).

2.4 Result

Four rounds of construct optimization were performed, and 25 constructs were screened (Table 2.1). In each round of optimization, constructs were expressed by the

same batch of insect cell to avoid inconsistence from different batches of insect cell, and all the biomass was purified at the same time as well.

Table 2.1

Histamine 4 Receptor Constructs

Construct ID	Truncation	Fusion (Ins. Position)	Mutation
1	/	/	/
2	H206-H292	D205-T4L-V293	/
3	H206-H292	D205-Bril-V293	/
4	H206-H292	D205-mT4L-V293	/
5	M1-N5/H206-H292	D205-Bril-V293	/
6	M1-L10/H206-H292	D205-Bril-V293	/
7	H206-H292/P381-S390	D205-Bril-V293	/
8	H206-H292/I375-S390	D205-Bril-V293	/
9	S208-H288	L207-Bril-Q289	/
10	H206-R290	D205-Bril-E291	/
11	C210-R290	R209-Bril-E291	/
12	C210-H288	R209-Bril-Q289	/
13	H206-H288	D205-Bril-Q289	/
14	C210-H292	R209-Bril-V293	/
15	S208-H292	L207-Bril-V293	/
16	D205-E291	R204-Bril-H292	/
17	D205-Q289	R204-Bril-R290	/
18	L207-E291	H206-Bril-H292	/
19	H206-E291	D205-Bril-H292	/
20	H206-Q289	D205-Bril-R290	/
21	D205-R290	R204-Bril-E291	/
22	L207-R290	H206-Bril-E291	/
23	D205-Q289	R204-Bril-R290	A298E
24	D205-Q289	R204-Bril-R290	R112A
25	D205-Q289	R204-Bril-R290	R112A, A298E

2.4.1 First Round Optimization: Fusion Protein Screening at ICLIII

The purpose of the first-round construct optimization is screening the fusion proteins at ICLIII that predominately used in GPCRs crystallization. Since the effect of where the fusion proteins were inserted is unpredictable, the junction site of the fusion proteins was determined by amino acid sequence alignment with one construct which was used to solve the structure of H1R. In this round, three fusion proteins were used to replace the same segment of ICLIII of histamine 4 receptor, T4L, Bril and mT4L. Figure 2.1 shows the western blot result, only constructs with fusion protein Bril has an extremely faint band on the membrane. Since western blot is a sensitive assay, very few proteins could show signal one the membrane. Wild type and constructs with T4L and mT4L fusion barely showed on the membrane indicates the expression level of these constructs were too low to be used to produce enough protein for crystallization. Therefore, Bril was the best fusion protein among the three candidates and was used for further optimization.

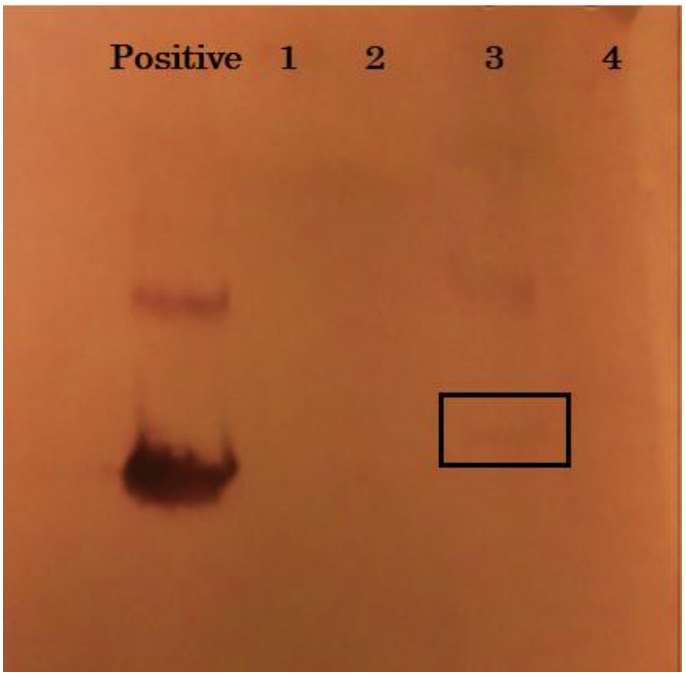

Figure 2.1 **Western-Bolt Result of First Round Optimization**. The faint band for was marked in the black frame showed on the membrane which represents the histamine 4 receptor monomer.

2.4.2 Second Round Optimization: N, C-termini Truncation Optimization

In this round optimization, 5 or 10 amino acid residuals were truncated at N and C termini respectively based on construct 3. N-termini play a crucial role in GPCRs' PTM such as glycosylation. Truncation of these glycosylation sites at N-termini could possibly destroy the correct folding or transportation of GPCRs. Both construct 5 and 6 have N-termini truncation which lead to a reduction of expression level, the more residuals were truncated, the less protein will be expressed. For the C-termini truncation, constructs 7 and 8 have lower expression level comparing with construct 3 without increasing the protein quality. In this round, construct 3 still perform

best, in other words, truncation at N, C-termini didn't help with either expression or quality. Based on the SDS-PAGE result (*Figure 2.2*) and High-Performance Liquid Chromatography (HPLC) result (*Figure 2.3*), the expression level was still too low because the band on the SDS-PAGE was faint and the absorbance of UV280nm was low.

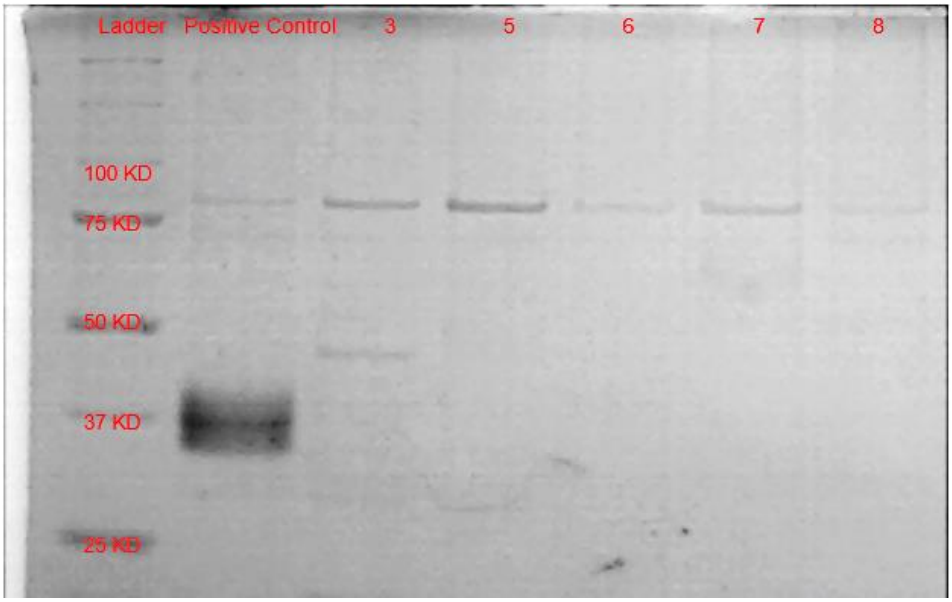

***Figure 2.2* SDS-PAGE Result of Second Round Optimization**. Only construct 3 showed a faint band at the correct molecular weight range.

A

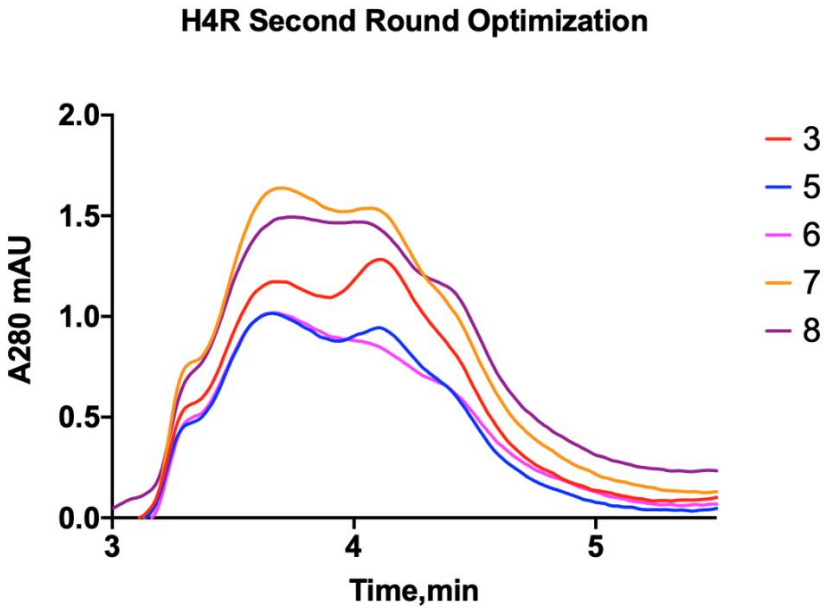

B

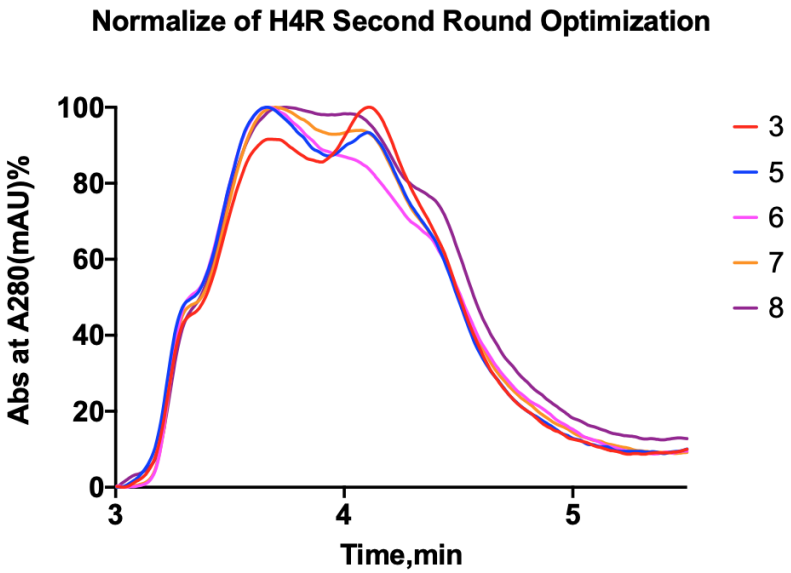

Figure 2.3 HPLC Result of Second Round Optimization. A showed the raw HPLC data for 5 constructs. Y-axis represented the absence of UV280nm, X axis

represented the retention time. B showed the normalized data which provided a better view of the comparing the homogeneity of the constructs.

2.4.3 Third Round Optimization: Junction Site Optimization

The third round optimization was based on construct 3 which has the highest expression level in first and second round optimization. In this round, the length of the linker on both left (the linker between fusion protein Bril and helix Ⅴ) and right (the linker between fusion protein Bril and helix Ⅵ) sides were optimized. The SDS-PAGE result (*Figure 2.4*) indicated that the expression level of couple constructs increased compared with wild type and construct 3. There was still impurity showed on the gel due to non-specific binding. *Figure 2.5* shows the HPLC curves of each construct. The peak showed around 4.5 min represented the monomer, and all the peaks came out earlier than that represented aggregation. Construct 17 was the best construct in this round because it has both relatively high yield and higher monomer population.

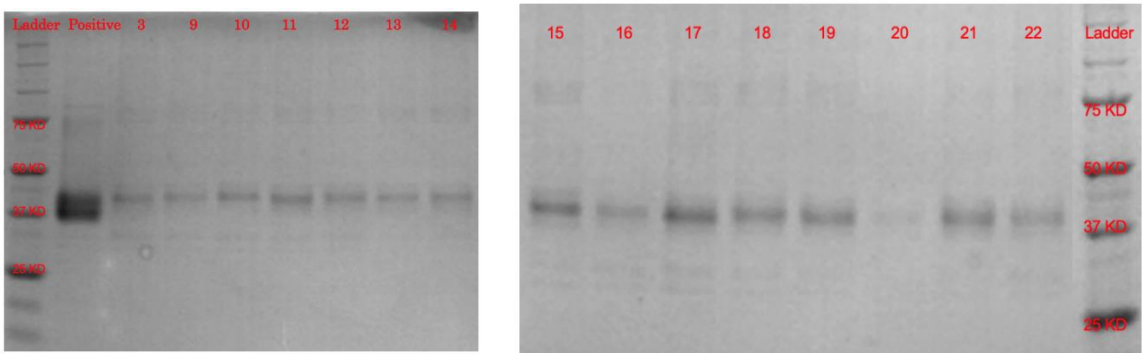

***Figure 2.4*. SDS-PAGE Result of Third Round Optimization**. Couple constructs showed higher expression level compared to construct 3.

A

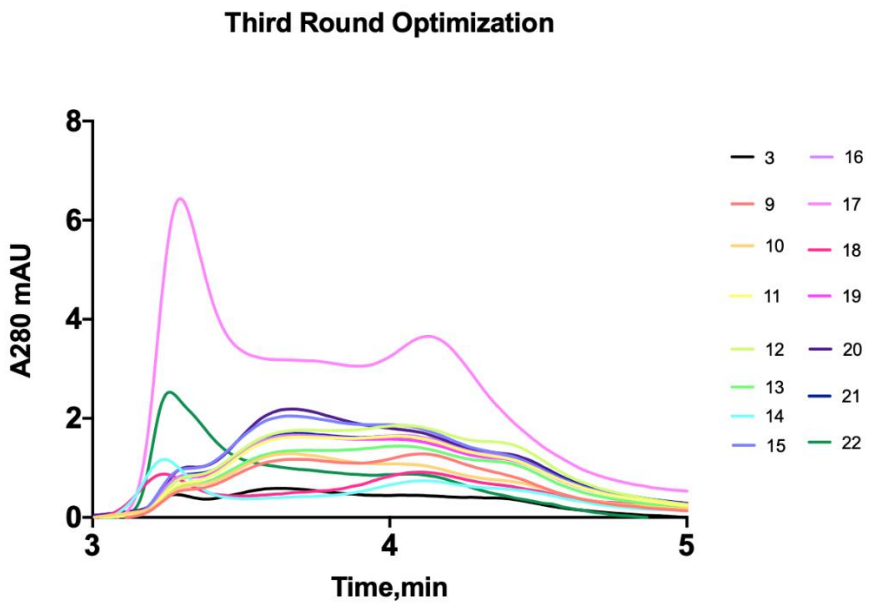

B

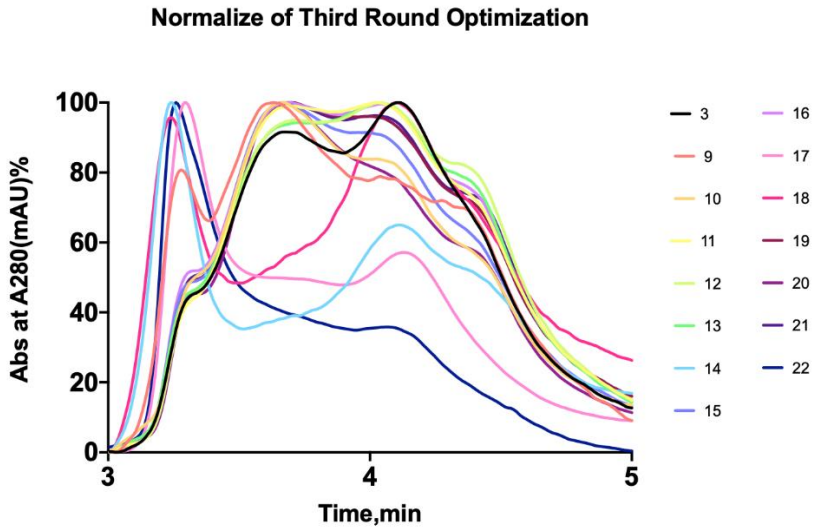

Figure 2.5 **HPLC Result of Third Round Optimization**. A showed the raw HPLC data for 15 constructs. Y-axis represented the absence of UV280nm, X axis represented the retention time. B showed the normalized data which provided a better view of the comparing the homogeneity of the constructs.

2.4.4 Fourth Round Optimization: Mutation Screening

Two mutations in the transmembrane bundle were tested in this round optimization based on construct 17. Construct 23 has mutation A298E, construct 24 has mutation R112A and construct 25 has double mutations (A298E, R112A). Based on the SDS-PAGE and HPLC result, both mutations could increase the protein expression level and protein homogeneity independently. However, the combination of these two mutations didn't make the construct better. Single mutation A298E performs best in this round.

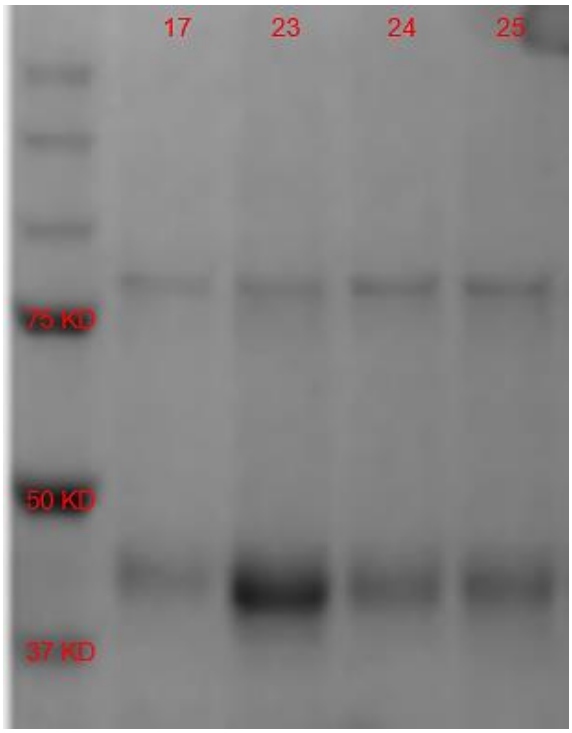

Figure 2.6. **SDS-PAGE Result of Fourth Round Optimization.** Construct 23 showed the highest expression.

A

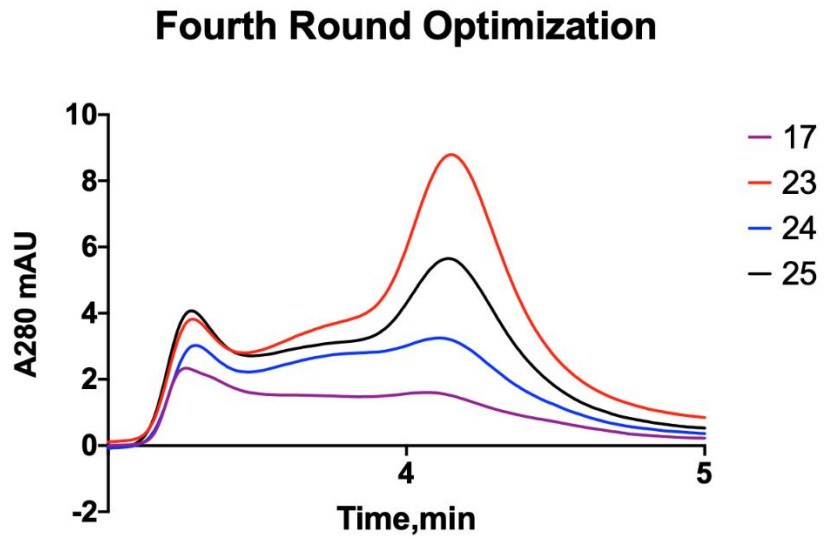

B

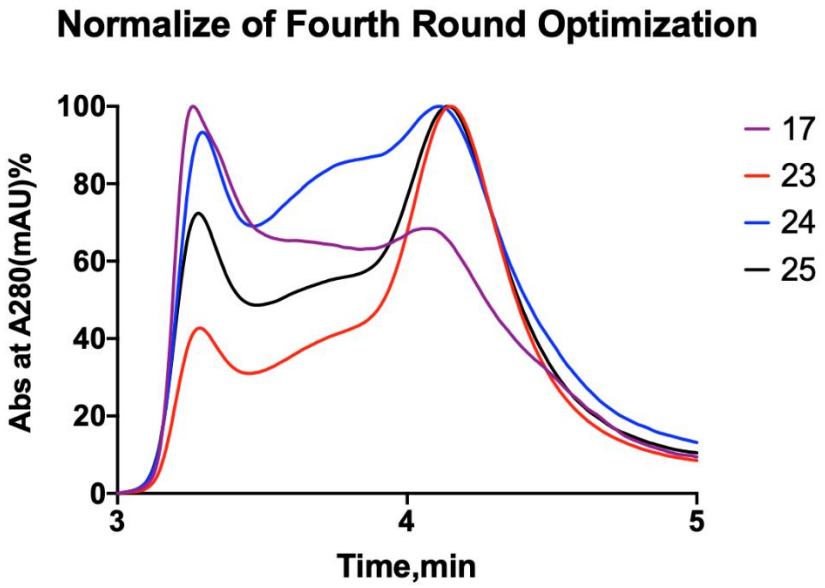

Figure 2.7 HPLC Result of Third Round Optimization. A showed the raw HPLC data for 4 constructs. Y-axis represented the absence of UV280nm, X axis represented the retention time. B showed the normalized data. Construct 17 which had A298E single mutation showed the highest homogeneity.

2.4.5 Ligand Screening

Construct 23 was selected to screen the ligand. It didn't show notable improvement on yield based on the SDS-PAGE data. Purifying with ligand slightly increased the protein thermostability, but the improvement is not significant, and the Tm value is still at a low range. It indicated the protein was over engineered. The A298E mutation may play an important role in ligand binding for H4R. Therefore, there is no notable difference between with or without ligand.

A

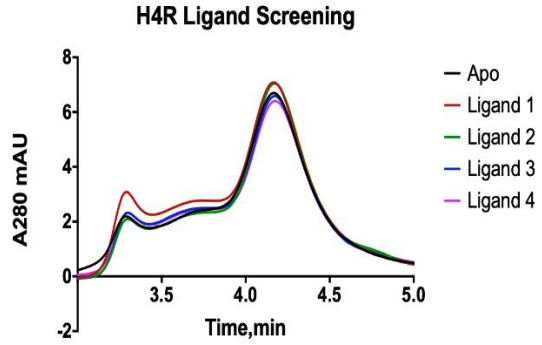

B

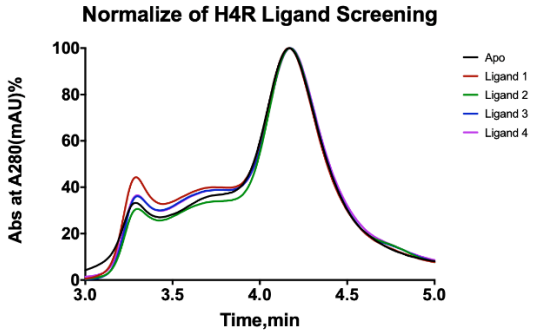

C

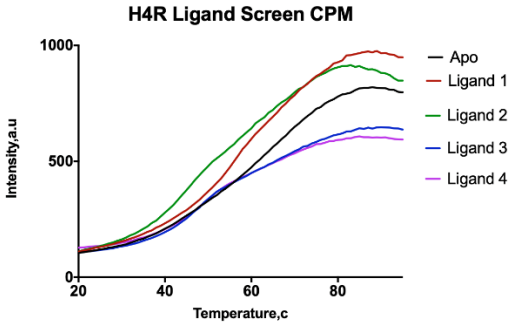

D

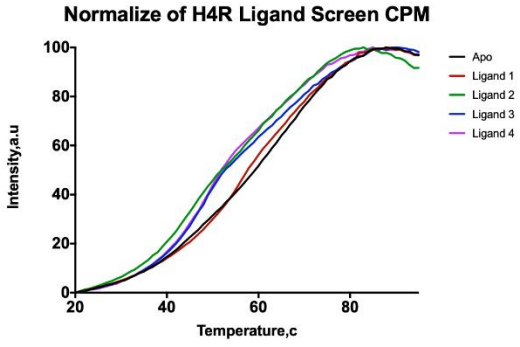

Figure 2.8. **Result for Ligand Screening**. A and B. HPLC result and normalized curves. C and D. Thermostability assay result and normalized curves.

Table 2.2

Tm Value for Ligand Screening

	Apo	Ligand 1	Ligand 2	Ligand 3	Ligand 4
Tm Value (Degree)	43.68	45.05	41.20	45.78	44.68

2.5 Discussion

After several rounds of construct optimization, the fusion protein, N, C-terminus truncation, junction site and mutations have been optimized. Only mutations increase the expression level and homogeneity of the protein notably. However, both mutations would destroy the ligand binding. That is why the path of crystallization stopped, because there is few GPCR crystallized without ligand. Ligand played a significant role in GPCR stabilization and homogenization, without ligand binding, the apo states GPCR would adopt multiple confirmation which is not preferable in protein crystallization process. But this project did not come to a dead end since several G protein-GPCR complex structures have been determined with cryo-electron microscopy(cryoEM). One bottleneck for cryoEM is the limitation of molecular weight of the macromolecules. The molecular wright of GPCR only usually below the limitation, but the complex can overcome the molecular weight limitation. Based on the published method and protocol, all the components needed for the complex formation including three G protein subunits and scfv16 which could stabilize the complex have been expressed and purified. The future for this project would be forming the H4R-G protein-scfv16 complex

and determine the structure using cryoEM. Because H4R needs to form complex with G protein, the ICL III of H4R cannot be replaced with fusion protein. Based on the previous expression data, the expression level of wild type H4R was extremely low, therefore some optimization might be needed. Based on the published result, inserting fusion protein at N termini could stabilize GPCR construct without blocking the complex formation. N termini fusion couple be a direction of optimization for H4R. Besides, the expression steps could be optimized as well. Infecting the insect cell with multiple viruses simultaneously that contain the genes of G protein and GPCR during the expression process might increase the expression level of H4R.

CHAPTER 3

STRUCTURE DETERMINATION FROM LIPIDIC CUBIC PHASE EMBEDDED MICROCRYSTALS BY MICROED

Adapted with permission from Lan Zhu, Guanhong Bu, Liang Jing et al. Structure determination from lipidic cubic phase embedded microcrystals by MicroED. *Structure*, *28*(10), 1149-1159.

3.1 Abstract

The lipidic cubic phase (LCP) technique has proved to facilitate the growth of high-quality crystals that are otherwise difficult to grow by other methods. However, the crystal size optimization process could be time and resource consuming, if it ever happens. Therefore, improved techniques for structure determination using these small crystals are an important strategy in diffraction technology development. Microcrystal electron diffraction (MicroED) is a technique that uses a cryo-transmission electron microscopy to collect electron diffraction data and determine high-resolution structures from very thin micro- and nanocrystals. In this work, we have used modified LCP and MicroED protocols to analyze crystals embedded in LCP converted by 2-methyl-2,4-pentanediol or lipase, including Proteinase K crystals grown in solution, cholesterol crystals, and human adenosine A2A receptor crystals grown in LCP. These results set the stage for the use of MicroED to analyze microcrystalline samples grown in LCP, especially for those highly challenging membrane protein targets.

3.2 Introduction

Structural determination of membrane proteins has been difficult primarily due to their low expression and low stability once isolated from their native membrane environment. Despite these difficulties, the number of membrane protein crystal structures has increased in recent years due to multiple technical break- throughs, including the lipidic cubic phase technique, which provides a lipid environment close to that of the native membrane protein environment. Since the first high-resolution bacteriorhodopsin structure from LCP was determined in 1997(Landau and Rosenbusch 1996, Pebay-Peyroula, Rummel et al. 1997), there are now over 120 unique membrane protein structures, covering a wide range of molecular sizes even to the bigger and bulkier proteins, resolved at atomic resolution from crystals formed in meso (Cherezov, Clogston et al. 2006, Li and Caffrey 2011, Aherne, Lyons et al. 2012, Caffrey, Li et al. 2012, Huang, Olieric et al. 2015, Li, Stansfeld et al. 2015, Vogeley, El Arnaout et al. 2016, Xiang, Chun et al. 2016, Ishchenko, Abola et al. 2017, Ishchenko, Peng et al. 2017, Johansson, Stauch et al. 2017, Ma, Weichert et al. 2017, Weinert, Olieric et al. 2017, Boutet, Fromme et al. 2018, El Ghachi, Howe et al. 2018, Huang, Olieric et al. 2018, Zabara, Chong et al. 2018, Jaeger, Bruenle et al. 2019, Lan, Lee et al. 2019, Weinert, Skopintsev et al. 2019, Winkler, Kidmose et al. 2019). However, one challenge with this technique is that when membrane proteins crystallize in LCP, the crystals are often very small microcrystals in the initial condition that cannot withstand the radiation damage during synchrotron X-ray diffraction data collection, and the crystal size optimization may take months to years without assurances of improved diffraction quality. Serial

femtosecond crystallography (SFX), which utilizes high-brilliance and ultra-fast X-ray pulses to capture single-crystal diffraction patterns from LCP- embedded membrane protein microcrystals before they are destructed, has recently been employed with great success (Liu, Wacker et al. 2013, Caffrey, Li et al. 2014, Weierstall, James et al. 2014, Johansson, Stauch et al. 2017, Boutet, Fromme et al. 2018, Nogly, Weinert et al. 2018, Stauch and Cherezov 2018). Nevertheless, the LCP-SFX technique is very time and resource intensive with limited experimental time because there are only six operational X-ray free electron laser facilities worldwide, currently. LCP serial crystallography technology has been successfully adapted for use with synchrotron radiation, with both monochromatic and polychromatic beamlines(Martin-Garcia, Conrad et al. 2017, Martin-Garcia, Zhu et al. 2019). Although this evolution provides exciting opportunities for structure determination from microcrystals, further developments are required to overcome existing hurdles. Moreover, serial crystallography methods require a very large number (in our experience, typically greater than 100,000) of microcrystal diffraction patterns to constitute a complete dataset for structure determination. Therefore, to improve the structural studies of important integral membrane proteins to resolve high-resolution details in a more high-throughput fashion, new methods for structure determination need to be developed for the small crystals grown in LCP.

The advent of a new technique, microcrystal electron diffraction (MicroED) in 2013, offers an alternative for the structure determination of proteins from microcrystal samples (Shi, Nannenga et al. 2013). MicroED is a method that is used to collect electron diffraction patterns from sub-micrometer sized three-

dimensional crystals in the electron microscope (EM)(Nannenga and Gonen 2018). Microcrystals are deposited on EM sample grids followed by sample blotting, because electrons cannot penetrate thick samples. To ensure the sample remains hydrated in the vacuum of the EM and to reduce radiation damage, the samples are vitrified and kept at cryogenic temperatures. The continuous-rotation data collection strategy for MicroED allows multiple diffraction patterns to be recorded from one single crystal with an extremely low electron dose, resulting in a series of diffraction patterns that can be indexed, integrated, and processed with crystallographic data processing software without any prior knowledge of unit cell parameters or geometry (Nannenga, Shi et al. 2014). Since the initial implementation of MicroED, there have been further efforts to improve this method to deter- mine structures of proteins, peptides, and small organic molecules(Nannenga and Gonen 2016, Gruene, Wennmacher et al. 2018, Jones, Martynowycz et al. 2018, Gemmi, Mugnaioli et al. 2019, Nannenga and Gonen 2019, Levine, Bu et al. 2020).

In this work, our goal is to combine MicroED with LCP micro- crystallography methods (LCP-MicroED) to determine structures from microcrystals within the LCP matrix. Here, we report the first MicroED structures of a model soluble protein, Proteinase K, that has been embedded in LCP. In addition, we have demonstrated the approach is suitable for generating MicroED samples for crystals grown within LCP by collecting cholesterol MicroED datasets and diffraction patterns of a model G protein-coupled receptor (GPCR), human adenosine A2A receptor (A_{2A}AR).

Proteinase K had been used extensively as a model protein to generate samples for both MicroED and new LCP-based serial crystallography method(de la Cruz, Hattne et al. 2017, Martin-Garcia, Conrad et al. 2017, Hattne, Shi et al. 2018, Martin-Garcia, Zhu et al. 2019, Martynowycz, Zhao et al. 2019). Cholesterol crystals grown in LCP were used to elucidate the structure determination of small molecules by MicroED. A_{2A}AR was chosen as a model GPCR crystallized in LCP using previously published conditions that resulted in a high-resolution SFX structure as well as the structures determined by serial crystallography studies at synchrotrons (Batyuk, Galli et al. 2016, Martin-Garcia, Conrad et al. 2017, Martin-Garcia, Zhu et al. 2019). By treating the LCP samples with different reagents to lower the viscosity of the LCP, we further optimized two strategies: dilution using MPD and treatment of the sample with lipase, which led to high-quality MicroED samples. Both strategies were used on the LCP-Proteinase K samples to successfully determine the structure of Proteinase K at 2.0 Å resolution using MicroED. Diffraction datasets collected from MPD-treated cholesterol crystals and A_{2A}AR crystals diffracted to ~1 Å and 4.5 Å , respectively. Cholesterol diffraction data were processed, with unit cell parameters matching previously known cholesterol crystals (Varsano, Beghi et al. 2018), and maps from the low-completeness datasets were generated. We also observed that the A_{2A}AR diffraction pattern is consistent with previously published results(Batyuk, Galli et al. 2016, Martin-Garcia, Conrad et al. 2017, Martin-Garcia, Zhu et al. 2019).

3.3 Results

Although LCP crystallization has achieved significant success in the structure determination of membrane proteins, due to the intrinsic high viscosity of the LCP matrix (Caffrey and Cherezov 2009), this technique is not well suited to standard MicroED sample preparation protocols. In order to identify sample preparation conditions and protocols that would allow MicroED to be used on samples embedded in LCP, we chose the well-studied model proteins, Proteinase K and A2AAR, as well as a small-molecule cholesterol, which have previously been used to benchmark both new LCP-based X-ray diffraction (Batyuk, Galli et al. 2016, Martin-Garcia, Zhu et al. 2019) and MicroED methods(Hattne, Shi et al. 2016). Proteinase K microcrystals were grown in a batch and re- constituted into the LCP to be used for further studies on LCP sample preparation for MicroED. As an initial test for crystals that were grown within the LCP matrix rather than embedded after crystal growth, cholesterol was crystallized in LCP, and MicroED data were collected on these crystals. Finally, A2AAR microcrystals were grown in LCP and directly treated for LCP- MicroED sample preparation, and single diffraction patterns were collected.

3.3.1 LCP Sample Conversions for EM Grid Deposition

We initially focused on the identification and optimization of sample preparation conditions that would allow the collection of MicroED data from crystals embedded or grown in LCP. Because the viscosity of the LCP matrix is too high to be directly deposited on EM grids and effectively blotted thin enough to be penetrated by the electron beam, we adapted two different strategies to reduce

the viscosity: (1) by mixing with certain additives to convert into a less viscous liquid analog of cubic phase, which could be a sponge phase(Qiu and Caffrey 2000, Caffrey 2015); (2) treatment with lipase to hydrolyze matrix lipids and convert LCP into a two-liquid phase system of water/glycerol solution and oleic acid(Nollert and Landau 1998, Nollert, Navarro et al. 2002).

First, we screened the following additives at various concentrations: 2-methyl-2,4-pentanediol (MPD), PEG200, PEG400, Jeffamine M600, t-butanol, ethylene glycol, and 1,4-butanediol (Wadsten, Wohri et al. 2006, Caffrey and Cherezov 2009). These seven agents are commonly used in traditional protein crystallization screening and cryoprotection solutions. Although previous studies have proposed that a less viscous lipid mesophase might form with the addition of these additives (Wadsten, Wohri et al. 2006, Liu, Chun et al. 2012), the condition of utilizing them to liberate crystals from the LCP matrix was not well defined. Initial tests were conducted with blank LCP by mixing the host lipid monoolein (MO) and Proteinase K precipitant buffer without protein. All seven additives could convert the blank LCP to a less viscous lipid mesophase in syringe mixing, in the range of 6%–18% with MPD, 24%–40% with PEG200, 32%–48% with PEG400, 9%–20% with Jeffamine M600, 11%–20% with t-butanol, 15%–33% with ethylene glycol, and 28%–41% with 1,4-butane- diol, consistent with previous sponge phase transition studies(Wadsten, Wohri et al. 2006).

We then tested the absorption of the resulting less viscous lipid mesophase on

blotting paper, in order to empirically determine how to blot these converted LCP samples to generate a thin layer sample suitable for vitrification for MicroED. In this step, samples were expelled out of the mixing syringe and deposited on the blot- ting paper, without external blotting force applied. Compared with the LCP droplet Figure 3.1 A), which retained its shape and did not blot on the filter paper, the seven additive-converted less viscous lipid mesophase samples showed absorption on the filter paper (Figure 3.1 B–1H). MPD-converted Figure 3.1 B) shows the most significant blotting relative to the other additive-converted samples. When similar blotting tests were conducted on EM grids, the MPD-converted lipid mesophase samples produced the most consistently thin samples for successful transmission electron microscopy (TEM) visualization. Therefore, MPD was selected for further experiments with Proteinase K, cholesterol, and A_{2A}AR crystals embedded in LCP.

In addition to the additive treatment to convert LCP to less viscous lipid mesophases, we investigated an alternative strategy by treating LCP with lipase to hydrolyze the host lipid molecules and transition the cubic phase to a two-liquid phase system(Nollert, Navarro et al. 2002). Blank LCP was again used to find an optimal hydrolysis ratio of LCP to lipase, as well as the minimum treatment time to completely separate LCP into two liquid phases. The LCP sample was expelled from the syringe mixer into a 0.2 mL microfuge tube, and freshly prepared lipase solution at 50 mg/mL was directly added on top of the LCP sample without additional pipet- ting. It was found that after a 14-h treatment in a 1:1 ratio of LCP and freshly prepared lipase solution incubated at

20oC, the solid cubic phase (Figure 3.1 I) was completely separated into two liquid layers (Figure 3.1 J). This lipase hydrolyzed sample also penetrated the blotting paper without any visible LCP residua on the surface (Figure 3.1 K). For those protein targets that do not require lipid molecules involved in crystal packing, this enzymic release method can be used to clean the LCP matrix for crystal liberation. As with the MPD-treated samples described above, this strategy was then tested with LCP-Proteinase K crystal samples to study crystal survival and grid preparation for data collection.

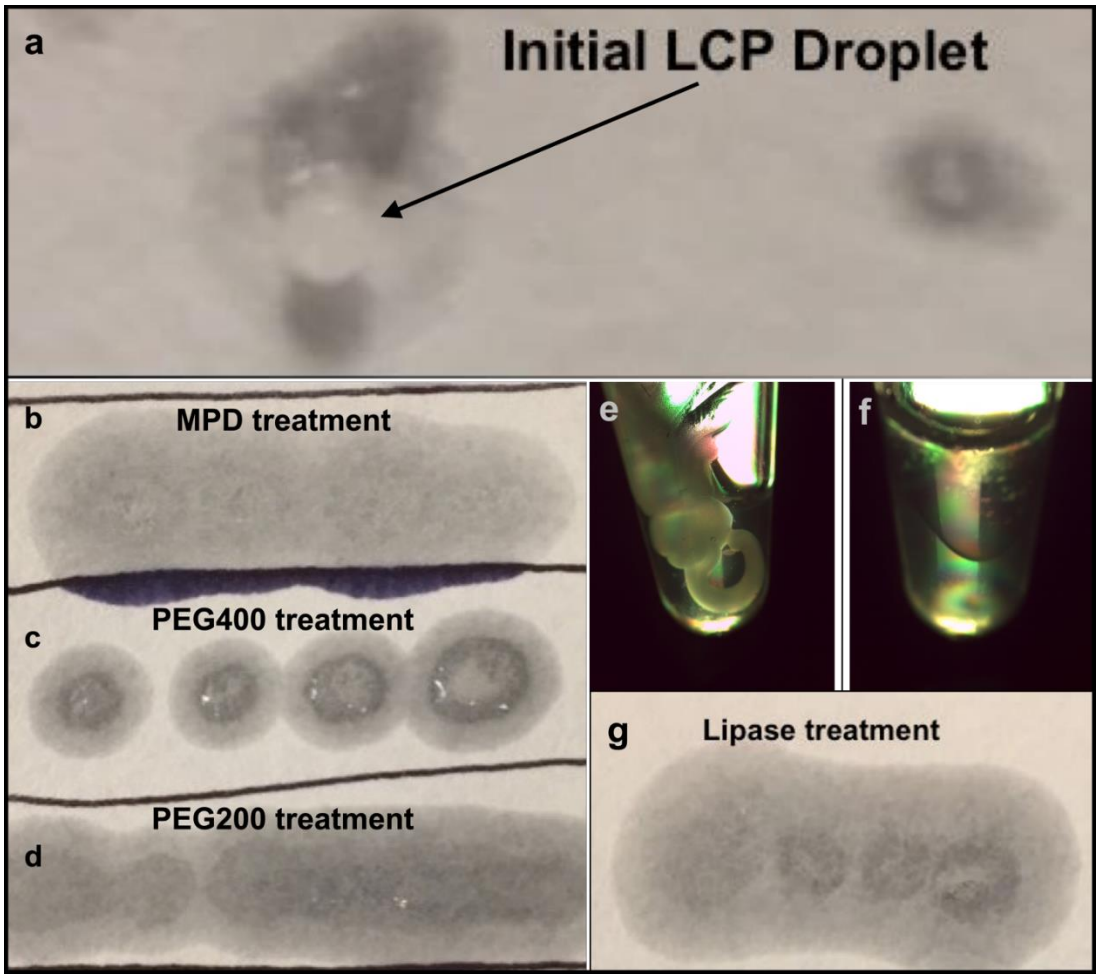

Figure 3.1 **LCP Phase Conversion.** LCP phase converting by the addition of spongifiers or the lipase treatment to generate low-viscous liquid-like sample

suitable for MicroED grid preparation. a) high-viscous LCP sample could not penetrate the blotting paper, rather to stay on the paper surface as a solid droplet. b-c) the treatment with the phase converting buffer supplemented with three spongifiers, MPD (b), PEG400 (c), and PEG200 (d), respectively, converted the LCP sample to a liquid-like phase, which penetrated the blotting paper. e-g) the lipase hydrolysis treatment of LCP sample to form two liquid phases, e) the LCP stream (white solid stream in the tube) with freshly prepared lipase solution mixed in a ratio of 1:1 (v/v) before treatment, f) the LCP sample was separated into two liquid phases after 14-hour treatment; g) the lipase hydrolyzed sample penetrated the blotting paper without LCP residue on the paper surface.

3.3.2 Microcrystal Survival During LCP Conversion

We then followed the batch crystallization method to grow Proteinase K microcrystals in solution (crystal size may range between 5 and 100 μm as shown in Figure 3.2 A, but only crystals<5 μm in size and ~0.5 μm thick would be targeted for MicroED data collection as in Figure 3.3 A and Figure 3.3 E) and reconstituted them into LCP (Figure 3.2 B) by dual-syringe mixing with the host lipid monoolein in a lipid: crystal solution ratio of 3:2 (v/v). Proteinase K microcrystals survived reconstitution into LCP B) and were used for the phase conversion test with MPD or lipase treatment.

For phase conversion, we tested MPD supplementation in the Proteinase K

precipitant solution with a range of 6%–18% MPD in 0.5% increments as a phase-converting buffer. This conversion buffer was then mixed with LCP-Proteinase K in the syringe. We observed that the converting buffer supplemented with more than 12.5% MPD resulted in fewer/no Proteinase K microcrystals or crystals with dissolved edges (crystal image not shown). Therefore, 12.5% MPD was chosen as the maximum concentration capable of reducing the viscosity of the LCP sample (Figure 3.1 B) without dissolving the embedded Proteinase K crystals (Figure 3.2 C).

LCP-Proteinase K samples were treated with lipase (1:1 v/v ratio) along with additional crystallization precipitant solution added as a supplement to ensure the stability of the Proteinase K crystals after release from the LCP. Lipid hydrolysis was monitored every 1 h for the first 14 h, and every 20 min afterward. After 18-h of lipase treatment, the sample composed of a 1:1:2 (v/v/v) ratio of lipase:LCP-Proteinase K: precipitant solution was completely hydrolyzed and separated into two liquid layers with the Proteinase K crystals being released from the LCP matrix into the glycerol-rich phase. We observed that the liquid phase contained crystals of similar size and density to that of Proteinase K microcrystals in the LCP-Proteinase K sample before the treatment (Figure 3.2 D).

With these sample preparation methods, the low-viscosity LCP-microcrystal solution was applied to glow-discharged carbon-coated EM grids, blotted with filter paper, and vitrified in a method similar to that used to prepare EM grids

for non- LCP-MicroED samples (Shi, Nannenga et al. 2016). The MPD-induced less viscous lipid mesophase sample was further diluted by adding the converting buffer in a 1:1 (v/v) ratio, which generated a thin layer on the EM grid where crystals could still be identified by UV microscopy (Figure 3.2 E). Lipase treatment also produced grids with a similar level of microcrystals visible by UV (Figure 3.2 F).

To further test the viability of the sample treatment strategy for crystals grown in LCP, cholesterol and the membrane protein A2AAR were crystallized in LCP and then examined using the MPD treatment method. A cholesterol- or A2AAR-laden LCP sample was crystallized in the presence of 28% PEG400 in the initial crystallization precipitant solution, which trans- formed the cubic phase into a less viscous intermediate phase. Once crystals formed to the size of the 2–3 µm needle shaped for cholesterol(Figure 3.4 A) and ~ 5 × 5 × 2 µm 3 for A_{2A}AR(Figure 3.5 A), excess precipitant solution was removed, and only 7% MPD was needed to convert the LCP by syringe mixing in a gentle manner. Further dilution by adding the converting buffer was applied before depositing crystals on the EM grid. A2AAR crystals on the grids were shown to have survived the addition of 7% MPD and the deposition process via UV microscopy (Figure 3.5 B). The diffraction quality of the A2AAR microcrystals following LCP conversion was also examined by X-ray diffraction using a microfocus beamline. These crystals retained their diffracting power to 2.4 Å resolution (Figure 3.5 E), indicating the treatment with MPD does not significantly reduce the crystal quality.

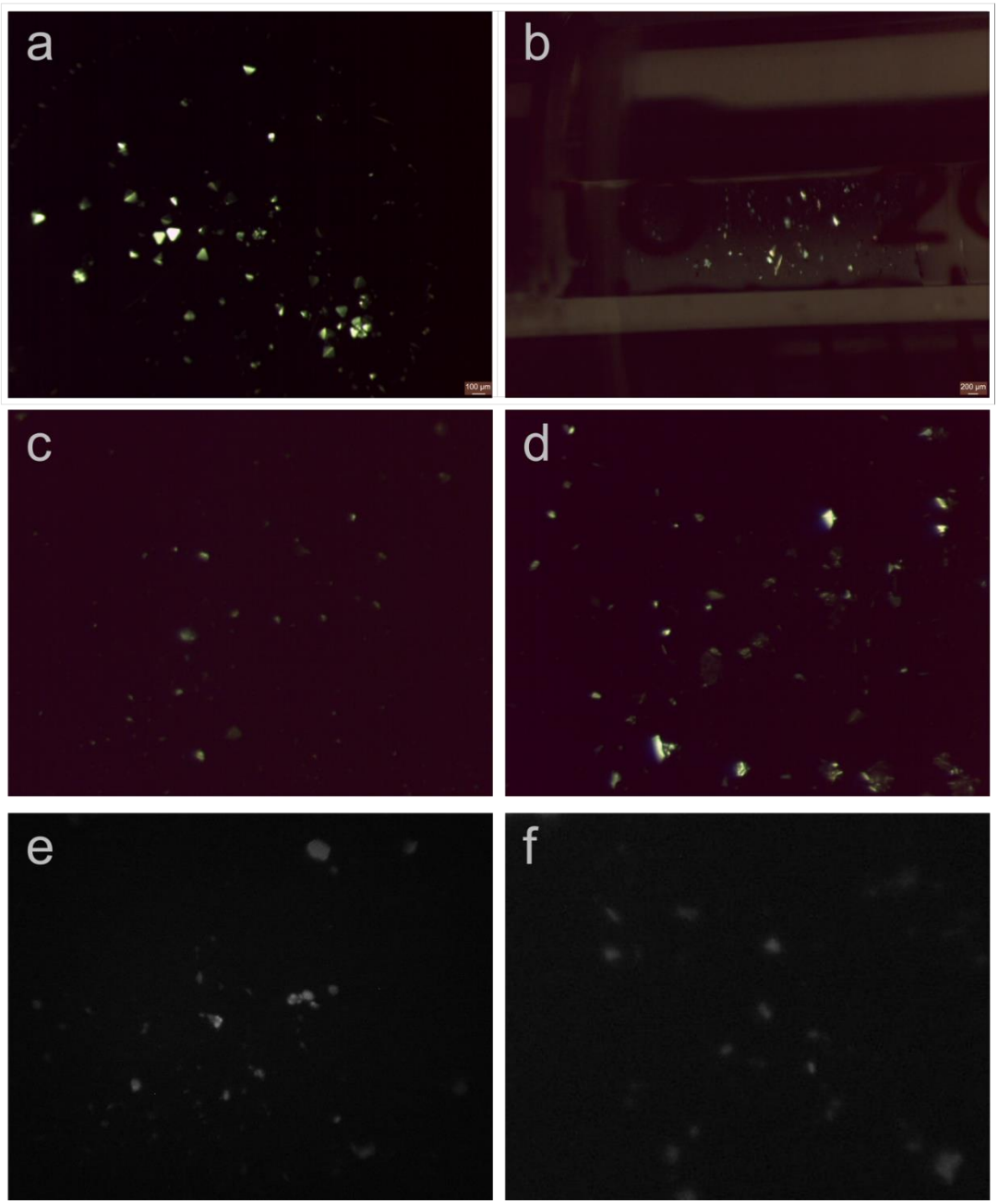

Figure 3.2 **Proteinase K Microcrystals Phase Conversion**. Proteinase K microcrystals were imaged before and after LCP phase converting. Microcrystals of proteinase K grown in batch method (a) and reconstituted into the LCP matrix by syringe mixing (b), viewed with cross polarizer light. Proteinase K

microcrystals embedded in LCP survived after the LCP phase converted by the converting buffer supplemented with 12.5% MPD (c) or LCP hydrolyzed by the lipase treatment (d), viewed with cross polarizer light. MPD-induced phase converted LCP-proteinase K microcrystal sample (e) and lipase treated LCP-proteinase K microcrystal sample (f) were successfully blotted on the glow-discharged EM grids used for MicroED data collection, viewed with UV light.

3.3.3 MicroED Analysis of Converted LCP Samples

Samples prepared by the methods described above were visually analyzed using cryo-TEM to verify the thickness and the presence of microcrystals. In all cases, regions of sample grids containing Proteinase K (Figure 3.3 a and e), cholesterol (Figure 3.4 A), or A_{2A}AR microcrystals (Figure 3.5 C) could be visually identified and confirmed.

In the case of Proteinase K, while both treatment strategies produced suitable samples, lipase-treated samples generally gave a thinner layer on the EM grid relative to the MPD-induced less viscous lipid mesophase samples. Standard MicroED diffraction screening, data collection, and data processing protocols (Hattne, Reyes et al. 2015, Shi, Nannenga et al. 2016) were used to collect high-resolution datasets from each type of sample preparation. For the MPD-converted samples, diffraction data from four Proteinase K crystals were merged together to produce a final dataset with a refined structure at 2.0 Å . In the case of the lipase-treated LCP samples, data from two crystals were used to resolve the structure of Proteinase K to 2.0 Å. Both of these methods of LCP sample

preparation ultimately produced high- quality MicroED data, density maps, and models (Table 3.1; Figure 3.3).

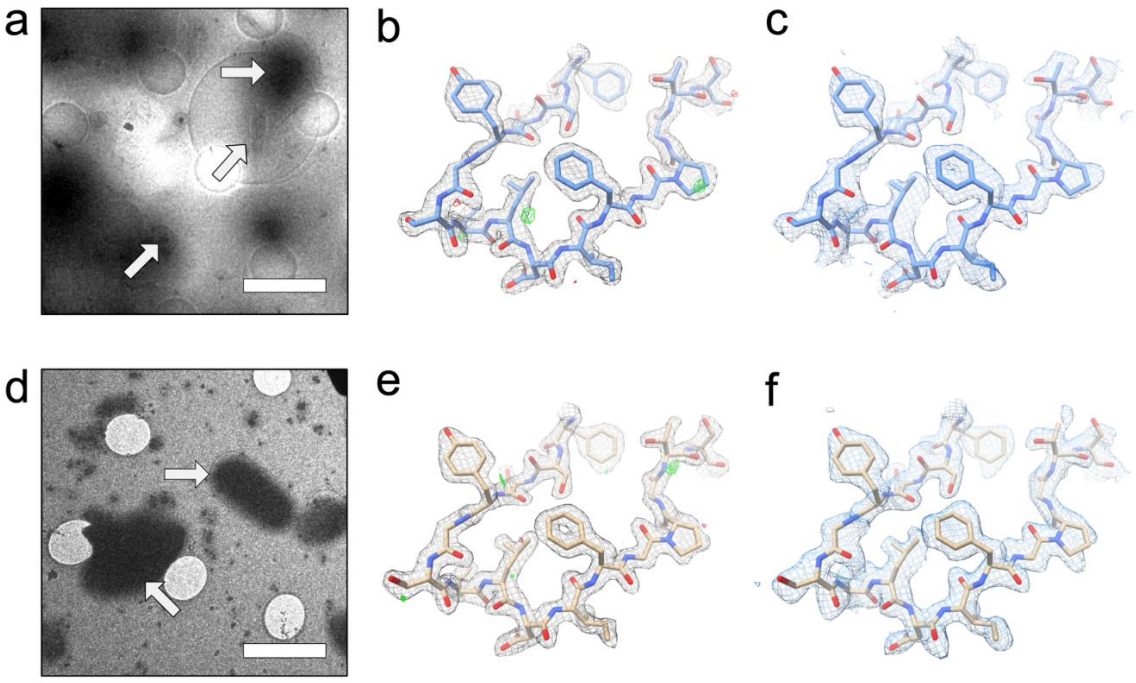

Figure 3.3 **LCP-MicroED structure of proteinase K**. Both MPD treated samples (a-c) and lipase treated samples (d-f) produced grids where crystals could be identified (a - MPD and d - lipase). MicroED data collection on these crystals from both treatments produced structures at 2.0 Å. The 2Fo-Fc density maps (b – MPD and e – lipase) and composite omit maps (c – MPD and f – lipase) show clear density surrounding the models. The density maps in b and e and composite omit maps in c and f are contoured at 1.5σ and 1.0σ, respectively. The 2Fo-Fc map in b and e is contoured at 3.0σ (green) and -3.0σ (red).

When compared with other Proteinase K structures deter- mined by MicroED (Hattne, Reyes et al. 2015, de la Cruz, Hattne et al. 2017, Hattne, Shi et al.

2018), both of the LCP-Proteinase K structures in this work showed similar levels of data quality (e.g., resolution, R factors), indicating that the LCP phase conversion method—whether induced by MPD or lipase—did not greatly impact the quality of vitrified crystals. In addition, the overall root-mean-square deviation (RMSD) is 0.59 Å between both of our models and another MicroED Proteinase K structure (PDB:5I9S;(Hattne, 2016 #82)), showing minimal differences. When we compare the MPD- and lipase-treated structures, the all-atom RMSD between these two new structures is 0.47 Å.

Cholesterol microcrystals grown in LCP were converted to a less viscous phase using the same protocol involving MPD. The vitrified sample on the EM grid (Figure 3.4 A) was diffracted using cryo-TEM, and subsequent diffraction patterns showed well-resolved spots to high resolution (slightly beyond 1 Å)(Figure 3.4 B).We were able to index the cholesterol datasets with a resulting P1 space group with unit cell dimensions of 12.257 Å ,12.343 Å , and 34.262 Å with angles of 89.551°, 83.497°, and 78.907° (Table 3.2.B). These values are consistent with previously published results on cholesterol structure (Craven 1976, Varsano, Beghi et al. 2018). Also, the X-ray structure of this cholesterol form (Craven 1976) was used to calculate model amplitudes, and they compared very well with the corresponding amplitudes obtained by MicroED (CC = 84.2%). Unfortunately, because of the low symmetry of the cholesterol crystals (P1) and the preferred orientation on the grid, the completeness of the merged dataset was very low (31.1%), which prevented the use of direct methods for phasing. Due to low data complete- ness, a reliable structure of cholesterol could not be

determined, however a projection map could be calculated. By using the X- ray model of cholesterol and molecular replacement, a projection map was generated that shows good maps when viewed along the direction containing high data completeness for the cholesterol and water molecules in the crystals (Figure 3.4 C). This is an important step because it demonstrated that the method used for the Proteinase K samples previously could also be extended to the collection of MicroED data from crystals that had been grown in LCP.

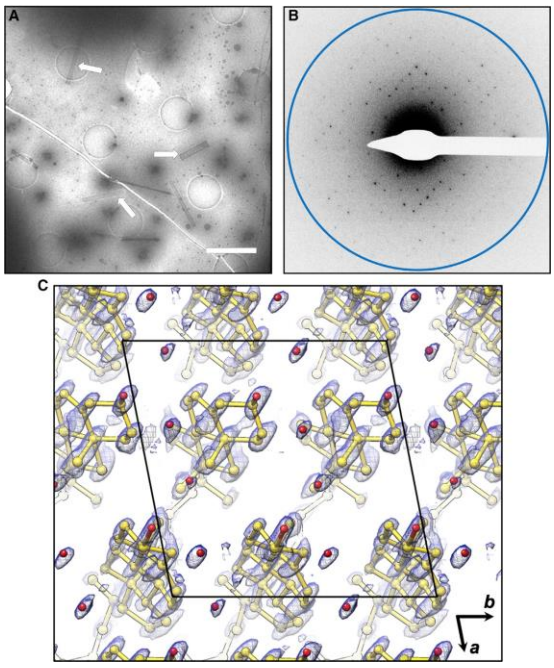

Figure 3.4 **Cholesterol Microcrystals and MicroED Diffraction** (A and B) After phase conversion with MPD, cholesterol microcrystals were located on the EM grids (A) and a still electron diffraction pattern was recorded with a resolution ring of 0.9 Å (B) before the continuous-rotation MicroED data collection in cryo-TEM. (C) The model and density map derived from the LCP-MicroED cholesterol data viewed along the direction with high completeness. Scale bar in (A) represents 3 mm.

We next applied the same MicroED data collection process to study $A_{2A}AR$ microcrystals and observed the diffraction to be about 4.5 Å (Figure 3.5 D). Although fewer spots were found in the diffraction patterns within a narrow tilt angle series, we were able to collect a small tilt series that showed the unit cell parameters are consistent with previously published A2AAR models, including one from LCP-SFX experiments (Batyuk, Galli et al. 2016).

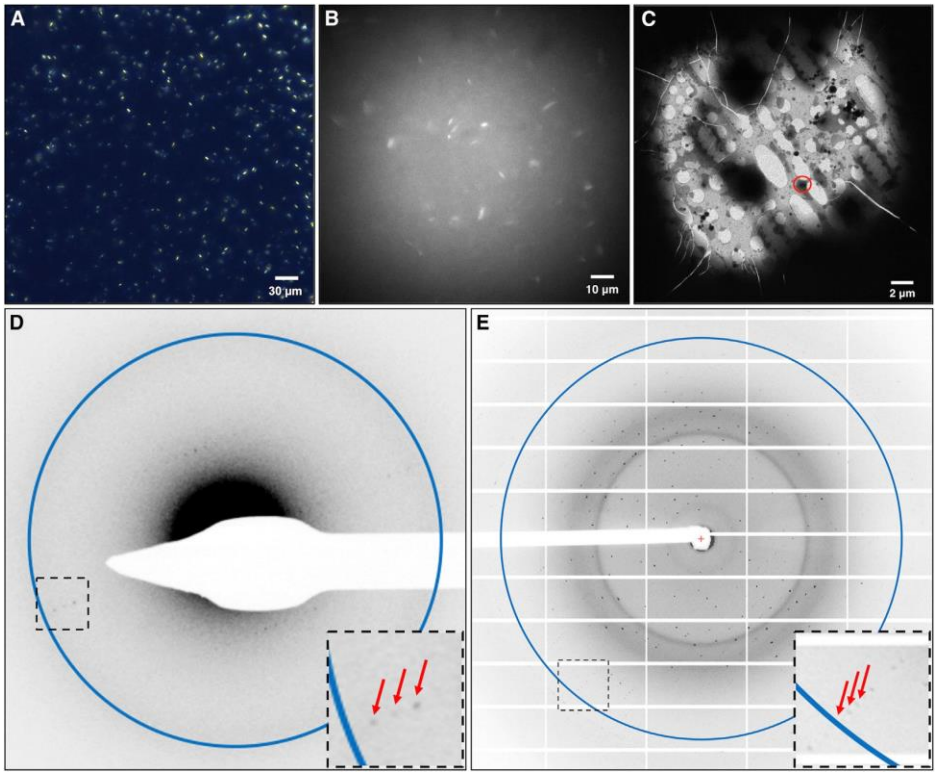

Figure 3.5 **$A_{2A}AR$ Microcrystal Monitoring and MicroED Diffraction.**
$A_{2A}AR$ was crystallized in LCP to a size of 5 × 5 × 2 μm^3 (A, viewed with cross-polarized light), and microcrystals survived after LCP phase conversion by the converting buffer supplemented with 7% MPD (B, viewed with UV). Microcrystals were located on the EM grids (C) and a still initial electron diffraction pattern with resolution ring of 4.5 Å (D) was recorded before the

continuous-rotation MicroED data collection in cryo-TEM. Red arrows denote the diffracted spots to 4.5 Å in a closer view of the black boxed area.
(E) A2AAR microcrystals, treated with the same phase conversion method, retained their diffraction power to ~2.4 Å resolution (shown as the resolution ring in the image at a microfocus X-ray beamline (diffracted spots to the highest resolution were denoted by red arrows in a closer view of the black boxed area).

3.4 Discussion

These results demonstrate, for the first time, that microcrystals embedded in LCP can yield high-resolution data and structures using MicroED. This proof-of-concept study and methodology presented here paves the way for future LCP-MicroED applications for challenging membrane protein targets that only form micro- or nanocrystals. To expand the application of LCP-MicroED to these difficult targets, further development and optimization based on these initial methods need to be explored. Because every LCP-microcrystal sample is unique, the expansion of the method reported here into a suite of techniques will be important for its broad applicability. For the use of additives for phase con-version, a broader spectrum of chemicals should be investigated for LCP-MicroED. Certain polar solvents or other additives such as propylene glycol and pentaerythritol propoxylate, are commonly used in membrane protein crystallization precipitant solutions and can also be used as phase conversion additives. The identification of a suite of additives compatible with LCP-MicroED would allow users to choose chemicals already present in the

crystallization precipitant solution (or components with similar chemical properties). When screening new additives, two critical fac- tors—the viscosity of the chemical and the overall percentage needed to convert the phase—should be kept in mind. In this study, we found that MPD behaved much better than PEGs in microcrystal blotting on EM grids, which was attributed to its lower viscosity and lower concentration (6%–18%) required for phase conversion to a less viscous state. The intrinsic viscosity is not a parameter that can be tuned easily; however, these additives typically have a wide range of concentrations that can drive conversion to a less viscous lipid mesophase(Wadsten, Wohri et al. 2006). While screening additives, some chemicals may affect microcrystal quality at the concentrations required to trigger the desired phase conversion. Therefore, for novel additives, their effects on phase conversion and crystal quality should be carefully examined.

After phase conversion by the addition of additives, the diffraction quality of converted microcrystal samples could be evaluation in a microfocus X-ray beamline either with a cryogenic frozen sample or with the equipped LCP sample injector at room temperature in serial mode. Once the crystal diffraction quality is confirmed, vitrified EM grids can be loaded into a scanning electron microscope to assess the distribution of blotted crystals with the excess LCP residua prior to data collection in cryo- TEM. Under a certain circumstance when the conversion by additives might disrupt the crystal diffraction quality, a lower concentration of additives in a safe range to preserve the crystal integrity could be used to partially convert the phase to a relatively lower viscosity,

although not sufficient to produce a pure clean MicroED grid. The thickness of the vitrified grids could be further reduced to remove the excess LCP, generating desirable-sized lamellae, by cryo-focused ion beam (cryo-FIB) milling prior to MicroED data collection (Duyvesteyn, Kotecha et al. 2018(Martynowycz, 2019 #104, Martynowycz, Zhao et al. 2019)). This strategy has been applied to several structure determinations by MicroED without damage to the underlying crystal lattice. Following the Proteinase K crystal diffraction data and structure determination, we crystallized, transformed the phase of, and vitrified cholesterol microcrystals grown in LCP for further MicroED data collection. The purpose of collecting cholesterol crystal diffraction is 2- fold: (1) to establish that in the A_{2A}AR-LCP crystallization condition (containing 10% w/w cholesterol supplemented in the host lipid monoolein), the concentration of cholesterol could not crystallize, even with MPD-induced phase conversion; and (2) that very high-resolution can be obtained following LCP conversion. The cholesterol crystals diffracted to high resolution and were able to be indexed showing small unit cell dimensions, indicating that the crystals indeed were a small-molecule compound. Further, cholesterol crystallization in LCP occurred at a higher concentration (30% w/w for our samples) than that used for A2AAR-LCP crystallization, satisfying any concern that cholesterol may have crystallized and contaminated the final A_{2A}AR crystal sample.

In this study, we present LCP-MicroED diffraction images and processed data using A_{2A}AR microcrystals. A_{2A}AR is a model GPCR that had been used extensively in diffraction method development and validation, particularly in

cases of using LCP as a carrier medium, such as LCP-SFX (Batyuk, Galli et al. 2016) and LCP-SMX (Martin-Garcia, Conrad et al. 2017). A_{2A}AR was crystallized in LCP in a high (28%) concentration of PEG400, which resulted in average crystal sizes of 5 × 5 × 2 μm^3 as previously described for LCP-SFX data collection(Batyuk, Galli et al. 2016). Due to the high concentration of PEG400, the phase of the matrix was intermediate to that of cubic and sponge, therefore we empirically determined that 7% MPD was sufficient to reduce the viscosity of the matrix further for blotting and vitrification onto EM grids. We were able to visually confirm the presence of the A_{2A}AR crystals on the EM grids that retained the appearance and dimensionality as we had observed prior to the MPD- mediated conversion. Further, MicroED experiments recorded diffraction spots that were visible to approximately 4.5 Å(Figure 3.5 D). The indexed unit cell dimensions were similar to previously published results, suggesting that these are A2AAR diffraction patterns because no other protein crystals were blotted onto the grids at the time of experiment (with the exception of Proteinase K), and no other components of the LCP matrix could have possibly diffracted with such unit cell parameters.

The microfocus X-ray diffraction data show that the A2AAR crystals diffract well even after undergoing the treatment described here, whereas when analyzed by MicroED, the diffraction only extended to 4.5 Å . This suggests that the weaker diffraction seen by MicroED is not a result of the sample processing procedures, but rather due to other factors. The most likely reason for the reduced diffraction is because of the thickness and shape of the A_{2A}AR crystals. MicroED requires the crystals to be thin (on the order of a few hundred nanometers) for

the electron beam to penetrate and produce reliable diffraction data. When the crystals are thicker than 1 mm, as is the case for the A_{2A}AR crystals in this study, much of the beam is absorbed by the sample. In addition, while not a problem for Proteinase K, excess LCP surrounding the A_{2A}AR crystals could also increase the absorption of the electron beam. In the case of A_{2A}AR, the average crystal size seen is approximately $5 \times 5 \times 2\ \mu m^3$, which is too thick, and as the crystals become smaller, the ratio of length and width to thickness remains relatively consistent. For crystals on the grid that are thin enough for MicroED, the length and width are also greatly reduced, and therefore the total number of unit cells in the electron beam is low. As described above, the use of cryo-FIB milling offers a solution to this problem, where the larger and thicker crystals could be milled leaving thin lamella that still had a reasonable area for diffraction. Cryo-FIB milling alone is not sufficient for preparing samples from LCP because the LCP matrix would still be too thick to process by cryo-FIB.

Therefore, protocols such as those presented in this work would still be required as upstream sample preparation prior to further sample processing by cryo- FIB milling. We expect that in future work, A_{2A}AR microcrystals will be the model system used to further optimize MicroED data collection for LCP-embedded membrane proteins by streamlining the mesophase conversion and vitrification process, with higher throughput diffraction experiments using the TEM, as well as in data collection and processing.

Because lipase hydrolyzes the lipids that make up the LCP matrix, lipase

treatment generally provided thinner vitrified samples relative to MPD treatment, thereby increasing the area that was visible in the EM. It has been previously shown that lipase treatment of bacteriorhodopsin crystals could be performed without degrading the crystals (Belrhali, Nollert et al. 1999). In the case of some membrane protein crystallization, lipid molecules may interact with membrane proteins and mediate protein crystal packing(Hanson, Cherezov et al. 2008, Liu, Chun et al. 2012); and the lipase hydrolysis treatment method may cause deleterious effects to the target membrane protein crystals. Therefore, lipase treatment should be evaluated extensively for different membrane protein targets prior to LCP-MicroED studies.

The combination of the extraordinary properties of LCP and MicroED promises to facilitate the determination of high-resolution structures of challenging protein targets using crystals just a few sub-micrometers thick. These structural studies with MicroED could open the door to the identification of new structural information by improving resolution of poorly ordered samples(de la Cruz, Hattne et al. 2017), determining structures with minimal radiation damage(Hattne, Shi et al. 2018) and facilitating the modeling of charge within structures(Yonekura, Kato et al. 2015); LCP-MicroED has the potential to be a robust method, expanding the scope of MicroED to the challenging membrane proteins, such as GPCRs, that do not exclusively grow in solutions, but instead with the great success of LCP crystallization, to solve high-resolution structures from microcrystals grown in LCP. Another intriguing potential is to apply MicroED to the structural elucidation of small molecules, potentially

complementing other EM techniques in materials studies. The successful development and use of LCP-MicroED will add another important tool to the field of structural biology.

3.5 Material and Methods

3.5.1 Microcrystal sample Preparation

Proteinase K (catalog no. P2308, Sigma) was crystallized using batch crystallization method by mixing equal volumes of proteinase K solution at 40 mg/mL in 0.02 M MES pH 6.5 and a precipitant solution composed of 0.1 M MES pH 6.5, 0.5 M sodium nitrate, 0.1 M calcium chloride. Proteinase K microcrystals appeared after 20 min incubation at 20 ^{o}C (Martin-Garcia, Conrad et al. 2017). Microcrystals were pelleted by centrifugation at 500 g for 5 min, resuspended in the crystallization buffer, and then reconstituted into LCP by mixing with molten monoolein host lipid (catalog no. M7765, Sigma) in a lipid: solution ratio of 3:2 (v:v) using a dual-syringe mixer until a homogeneous and transparent LCP was formed(Caffrey and Cherezov 2009).

The mixture of cholesterol (catalog no. CH200, Anatrace) and monoolein in a ratio of 3:7 (w/w) was co-dissolved in chloroform, and solvent was removed by evaporation under a stream of an inert gas followed by high vacuum drying at RT for 24 hours. Cholesterol was reconstituted into LCP by mixing of the premixture with water in a ratio of 3:2 (v/v) and injected into a syringe containing the precipitant solution same as A_{2A}AR crystallization. Cholesterol

crystals formed in LCP stream after 18 hours incubation at RT.

A_{2A}AR was expressed, purified, and crystallized as described before(Liu, Chun et al. 2012, Liu, Ishchenko et al. 2014, Batyuk, Galli et al. 2016). In brief, the A_{2A}AR construct containing the BRIL fusion protein in intracellular loop 3 (A_{2A}AR-BRIL) was subcloned into the pFastBac1 vector and trans- formed into One ShotTM TOP10 competent *E.coli* cells. Recombinant A_{2A}AR bacmid DNA was prepared by transforming MAX EfficiencyTM DH10Bac competent cells, followed by transfection of Sf9 cells to generate A_{2A}AR baculoviruses. Sf9 cells were grown to 2 x 10^6 cells per mL before A_{2A}AR baculovirus was added for infection. A_{2A}AR was expressed in Sf9 cells for 48 hours at 27oC after infection, and cells were harvested by centrifugation and stored at -80^{o}C until purification. Once the protein was purified and concentrated to approximately 25 mg/mL, A_{2A}AR was reconstituted into LCP by mixing with molten monoolein, containing 40% (w/w) protein solution, 54% (w/w) monoolein and 6% (w/w) cholesterol. The protein-laden LCP were then injected into Hamilton gas-tight syringes containing precipitant solution composed of 28% (v/v) PEG400, 40 mM sodium thiocyanate, and 100 mM sodium citrate pH 5.0. A_{2A}AR microcrystals formed in LCP stream after 24 hours incubation at 20^{o}C. Upon further inspection, the A_{2A}AR microcrystals appear comparable to previously crystallized samples (Batyuk, Galli et al. 2016, Martin-Garcia, Conrad et al. 2017) in different microscopy imaging modes (Figure 3.5 A).

3.5.2 LCP Microcrystal Sample Conversion Set-up

Proteinase K microcrystals embedded in LCP were then either converted by mixing with additives to achieve a less viscous lipid mesophase or subjected to lipase treatment to separate into two immiscible liquid phases.
LCP-proteinase K crystal sample conversion was tested with seven additives, MPD, PEG200, PEG400, Jeffamine M600, t-butanol, ethylene glycol, and 1,4-butanediol. Sample conversion was performed by syringe mixing 15-20 times of an LCP embedded proteinase K sample in one syringe and the conversion buffer in the other syringe. The conversion buffer was made from the initial crystallization buffer supplemented with each of different additives. Each conversion buffer was optimized with a gradient additive concentration series of 10% increments. Finer additive concentration optimization followed when an initial point was identified that was capable of converting the LCP phase to a less viscous lipid mesophase. Once the concentration range of supplemented additive was identified, EM grid blotting experiments were conducted to investigate the capability of the additives for producing quality MicroED samples. Among those seven additives, only MPD-induced less viscous lipid mesophase sample exhibited reproducibly good quality EM grids. MPD was then focused for further optimization to ensure crystal survival during phase conversion. Once the LCP phase was converted, LCP-microcrystal samples were transferred into a microcentrifuge tube. Crystals were centrifuged and harvested from the bottom of the tube by pipetting. These samples were applied to a glass slide to monitor crystal survival by light microscopy with cross-

polarized and UV light or deposited on EM grid for analysis in the cryo-TEM. In the case of lipase treatment, LCP-proteinase K microcrystal samples were expelled from the LCP mixing syringe into a 0.2 mL microcentrifuge tube, followed by the addition of freshly prepared lipase solution at a volume ratio of 1:1:2 (lipase solution: LCP:crystallization buffer) directly into the same tube without mixing. The lipase used is from Candida rugosa (catalog no. L1754, Sigma) and is prepared at a concentration of 50 mg/mL in saturated K phosphate buffer. Incubation for at least 18 hours converts the lipidic cubic phase into a two-phase system consisting of two immiscible liquids: water/glycerol and oleic acid. Proteinase K crystals partitioned into the glycerol/water phase.

Once A_{2A}AR microcrystals formed in LCP stream, excess precipitant solution was removed from syringe and the LCP- A_{2A}AR crystal sample was directly used for MicroED sample preparation. LCP-A_{2A}AR crystal sample conversion was tested with four additives, MPD, Jeffamine M600, PEG200, and PEG400, by syringe mixing 3-5 times very gently with conversion buffer in the other syringe. Same as the conversion test of proteinase K, only MPD-treatment produced good quality EM grids with clear and thin window visualized in TEM. The conversion buffer was made from the initial crystallization buffer supplemented with 7% MPD. After syringe mixing of LCP- A_{2A}AR crystals with conversion buffer, sample was incubated at 20 ^{o}C for 10 min allowing the MPD better diffusing in the LCP matrix. Once the LCP phase was converted, no further dilution with conversion buffer was required for A_{2A}AR sample. X-ray crystallographic data on

converted $A_{2A}AR$ samples were collected on the 23ID-D beamline (GM/CA) of the Advanced Photon Source at the Argonne National Laboratory using a 5 um minibeam collimator following previous protocols (Liu, Chun et al. 2012). LCP-cholesterol crystal samples were converted with MPD treatment, following the same setup as stated above for $A_{2A}AR$.

3.5.3 MicroED Sample Preparation and Data Collection

After MPD or lipase treatment, proteinase K microcrystals were collected by centrifugation at 500 g for 5 min. Crystal solution was then harvested by pipetting from the microfuge tube bottom into a fresh microfuge tube. For MPD samples, the crystal solution was further diluted by adding a 1:1 ratio of fresh precipitant solution supplemented with 12.5% MPD. Cholesterol and A2AAR microcrystals were directly applied to a glass slide to monitor crystal survival by light microscopy with cross-polarized and UV light or deposited on EM grid for analysis in the cryo-TEM. Cryo-TEM samples were prepared by standard MicroED sample preparation procedures (Shi, Nannenga et al. 2016). Briefly, 2 μL of crystal solution was deposited on each side of a glow-discharged holey carbon EM grid (Quantifoil 2/4 for proteinase K crystals and cholesterol crystals, Quantifoil Multi A for A2AAR crystals), and the grid was processed with a Vitrobot Mark IV (Thermo Fisher) by blotting for 12-16 s followed by vitrification by plunging into liquid ethane. Sample preparation was optimized and screened in high-throughput fashion using a Titan Krios with CETA CMOS detector (Thermo Fisher). MicroED data collection of proteinase K was

performed by standard methods (Shi, Nannenga et al. 2016) using a FEI TF20 ~ cryo-TEM equipped with a F416 CMOS detector (TVIPS), operated at 200 kV. Diffraction data sets were collected as the stage was continuously rotated at a rate of 0.09 o/s and the detector collected frames every 4 s at a dosage of approximately 0.01 $e^-/Å^2$ per second. Data sets covered approximately a 45°, for a total dose of no more than ~5 $e^-/Å^2$ per data set. A_{2A}AR and cholesterol data collection were performed using a Titan Krios with CETA CMOS detector, operated at 300 kV, with continuously rotation at a rate of ~0.09 °/s and 0.91 °/s and the detector collected frames every 8 s and 2 s for A_{2A}AR and cholesterol crystals, respectively. Data sets from A_{2A}AR were collected to cover ~20° wedge, and those from cholesterol were collected to cover ~45o. The selected area aperture of the TEM was used to limit the area for single crystal from which data were collected.

3.5.4 MicroED Data Processing and Structure Determination

MicroED data collected from MPD and lipase treated LCP-proteinase K microcrystals were indexed and integrated in iMOSFLM (Battye, Kontogiannis et al. 2011). For each treatment, data from multiple crystals (4 for MPD-treated and 2 for lipase-treated) were merged and scaled in AIMLESS (Evans and Murshudov 2013) to create merged data sets with high completeness. Phaser (McCoy, Grosse-Kunstleve et al. 2007) was used to perform molecular replacement using a Proteinase K model (PDB ID: 2ID8, (Wang, 2006 #123)). The molecular replacement solution was refined using phenix. refine (Afonine,

Grosse-Kunstleve et al. 2012) using electron scattering factors, followed by manual inspection of the model in Coot(Emsley and Cowtan 2004, Emsley, Lohkamp et al. 2010). This process is then repeated iteratively with attention paid to avoid phase bias from the initial Proteinase K molecular replacement template (2ID8).

A_{2A}AR diffraction data were recorded as movie files of continuous tilt series. The images were extracted from the movie files first using the script mrc2tif from the IMOD software package(Kremer, Mastronarde et al. 1996, Mastronarde 2008); followed by the script tiff2smv from the TVIPS tools software suite(Hattne, Reyes et al. 2015) to generate images in formats that can be processed by standard X-ray diffraction processing software. Cholesterol datasets were converted using similar conversion tools (Hattne, Martynowycz et al. 2019). XDSGUI(Kabsch 2010) was used for subsequent spot picking, indexing, integration, and scaling of the diffraction data. Cholesterol data from two crystals were merged using AIMLESS, and a previous model of cholesterol (CSD Entry: CHOLES20) was used to phase the diffraction data with Phaser.

Table 3.1. Data Collection and Refinement Statistics

Data Collection

Excitation voltage	200 kV
Electron source	field
emission gun	
Wavelength (Å)	0.025079
Total dose per crystal	~4 e-/Å 2
Frame rate	4 s/frame
Rotation rate	0.09o/s

Data Processing

MPD-treated		Lipase-treated
Number of crystals	4	2
Space group	P43212	P43212
Unit cell dimensions		
a, b, c (Å)	67.4, 67.4, 106.5	67.6, 67.6, 106.8
a = b = g (o)	90	90o
Resolution (Å)	17.4–2.0	16.6–2.0
Total reflections	111,081	85,421

Total unique reflections	14,491	16,351
Rmerge (%)	32.4 (53.2)	40.4 (70.5)
CC1/2	0.937 (0.368)	0.900 (0.275)
Multiplicity	7.7 (6.3)	5.2 (5.4)
Completeness (%)	84.6 (63.3)	94.6 (94.8)
Mean (I/s(I))	5.5 (3.4)	4.0 (2.6)

Data Refinement

Rwork/Rfree (%)	21.7/26.7	24.4/28.2
RMSD bonds (Å)	0.003	0.003
RMSD angles (o)	0.571	0.478
Ramachandran (%) (Favored; allowed; outlier)	96.8; 2.8; 0.4	97.1; 2.9; 0

aValues for highest resolution shell of 2.05–2.0 Å .

bStatistics given by MolProbity

Table 3.2. Cholesterol Data Collection Statistics

Data Collection	
Excitation voltage	300 kV
Electron source gun	field emission
Wavelength (Å)	0.019687
Total dose per crystal	~2 e^-/Å 2
Frame rate	2 s/frame
Rotation rate	0.91o/s
Data Processing	
Number of crystals	2
Space group	P1
Unit cell dimensions	
a, b, c (Å)	12.257, 12.343, 34.262
a = b = g (o)	89.551, 83.497, 78.907
Resolution (Å)	1.00
Total reflections	8,582
Total unique reflections	3,293
Rmerge (%)	0.206 (0.835)
CC1/2	0.978 (0.393)
Multiplicity	2.6 (2.7)
Completeness (%)	31.1 (30.9)

aValues for highest resolution shell of 1.03–1.00 Å.

CHAPTER 4

STRUCTURE DETERMINATION OF ß$_2$- ADRENERGIC G PROTEIN COUPLED RECEPTOR BY MICROED

4.1 Abstract

Microcrystal electron diffraction (MicroED) utilized cryo-transmission electron microscopy to collect electron diffraction data from tiny crystals to determine high resolution structures. In recent years, it has achieved a great success with soluble proteins and small molecules, but the application of MicroED with membrane protein was hindered. Lipidic cubic phase (LCP) has shown its promising capability in membrane protein crystallization. However, as an essential sample preparation step, the high viscosity nature of LCP obstructs the application of the crystal embedded LCP on the EM grids for MicroED investigation. LCP-MicroED approach has been developed to convert crystal embedded LCP to less viscous sponge-like phase mixed with certain additives without sacrificing the protein crystal quality for electron diffraction data collection. In this research, we further applied the established protocol to a membrane protein target, ß2-adrenergic receptor(ß$_2$AR) and determined the 3.9 Å structure. This result further confirmed the feasibility of LCP-MicroED method as well as extending the scope of this method to the more challenging membrane protein targets.

4.2 Introduction

G protein coupled receptors were the target for more than 40 % drugs on the market due to the essential functions they performed in multiple physiological bioactivities in human body(Congreve and Marshall 2010). Determination of high-resolution protein structures of GPCRs would unveil deeper molecular mechanisms about protein function, as well as facilitating the rational drug design. During the past decades, high resolution structures of GPCRs were majorly solved by crystallography. However, the low expression and low stability natures of GPCRs made it very challenging to crystallize, there are only 105 unique GPCRs structures available so far according to the data from GPCR database(Velankar, Burley et al. 2021). The number of GPCR structures surged in the past 2 decades based on the application of lipidic cubic phase (LCP) into membrane protein crystallography. LCP is a mimic of lipid bilayer, which is the native environment that membrane proteins locate. The highly curved, bicontinuous natures of LCP make it an ideal crystallization medium for membrane proteins (Caffrey and Cherezov 2009). Nevertheless, the membrane proteins usually form small crystals in LCP which could not tolerate the radiation damage of X-ray generated from synchrotron source. X-ray free electron laser (XFEL) is one optimal alternative to collection high resolution diffraction data from small protein crystal. With the ultra-brilliant and femtosecond X-ray pulses, diffraction data could be recorded before the micron-sized protein crystals get destroyed. However, the accessibility of XFEL sources is very completive since there are only six XFEL facility worldwide (Zhu, 2020 #53).

The application of MicroED offers another alternative to collect diffraction from tiny crystals. MicroED utilized the electron microscope to collect the electron diffraction from the sub-micron-sized protein crystal deposited on the EM grids. The electron diffraction data could be processed by commonly used software for X-ray crystallography. Previous study determined the structure of proteinase K (PK) and cholesterol, which proved the feasibility of LCP-MicroED method (Zhu, Bu et al. 2020). Converting the LCP to less viscous sponge like phase won't reduce the quality of either protein crystals or small molecule crystals. The collection of adenosine A_{2A} receptor(A_{2A}AR) diffraction pattern indicated the LCP-MicroED method might work with GPCRs crystals that crystallized in LCP. However, due to the thickness problem while rotationally collecting the diffraction from A_{2A}R crystals, only few diffraction patterns were recorded which was insufficient to index.

In this study, we employed another well-studied GPCR target, $ß_2$-adrenergic receptor($ß_2$AR), to further confirm and develop the LCP-MicroED method. $ß_2$AR structure was first determined by X-ray crystallography at a synchrotron source (Cherezov, Rosenbaum et al. 2007). The ß2AR crystal in LCP was in a blade-like shape, the thickness of the two tips of the protein crystals might be thin enough to be penetrate by electron beam, which ensure the collection of the electron diffraction. ß2AR was widely used for multiple structure related research due to its high yield and stability. So far there are more than 30 $ß_2$AR structures available, which offers a great source for both data processing and data analysis.

The thickness of the crystal is always an obstacle for MicroED. Cryo-focused ion beam (FIB) is a technology which uses ion beam to melt the sample on the grid under cryo-environment (Martynowycz, Zhao et al. 2019). This technology could modify the crystal thickness to about 300 nm, which works optimally with electron diffraction. Because the size and shape of protein crystals are not controllable, cryo-FIB might offer a universal solution for the crystal thickness problem. However, the cryo-FIB instrument is not very affordable for most of the research institutions, and this process requires experienced technician to proceed which further decreases the accessibility of this technology. Besides, melting the protein crystal introduces extra artificial modification which might potentially change the crystal packing and lead to an over modified result. The advantages of LCP-MicroED method include simplicity and accessibility. The most essential process of the LCP-MicroED method is sample preparation. Direct converting LCP to less viscous sponge like phase by adding additive enables the deposition of protein crystals on the EM grid, which could be plunged and loaded directly to the electron microscope without any over artificial modification of the crystals such as Cryo-FIB. Recent years, the number of cryo-EM instrument and facility surged, which make LCP-MicroED method an accessible technology for more and more structure biologists.

4.3 Result

4.3.1 Low Completeness but Applicable with GPCR

The completeness of the β_2AR model built from MicroED data was 30 %-40 % which was lower than the boundary of typical completeness to determine a high-resolution

protein structure. Therefore, the model missed electron density for most of the side chain as well as the information about interaction among amino acids from different helixes. However, the backbone of the protein matched with the synchrotron diffraction structure (RMSD) and XFEL diffraction structure (RMSD) which indicated the feasibility of the LCP-MicroED method and protocol. It was worth to mention that this result further expanded the application of LCP-MicroED protocol. Previous study successfully determined the structure of PK whose crystals were reconstituted into LCP, as well as the structure of cholesterol, a small molecule whose crystals were crystallized natively in LCP. From A_{2A}AR, a membrane protein crystallized in LCP, only few unindexable diffraction patterns were collected. Even thickness of the A_{2A}AR crystal was believed the major reason of the poor diffraction quality, it was always a concern that the conversion of the phase during the sample preparation process might interrupt the protein-lipid interaction, if there was any, which could potentially jeopardize the crystal structure and diffraction. Notably, previous study has confirmed that $ß_2$AR formed interaction with cholesterol (Hanson, Cherezov et al. 2008), our MicroED data proved that the phase conversion won't hurt the crystal quality even for the GPCR targets that interact with lipid molecule.

A B

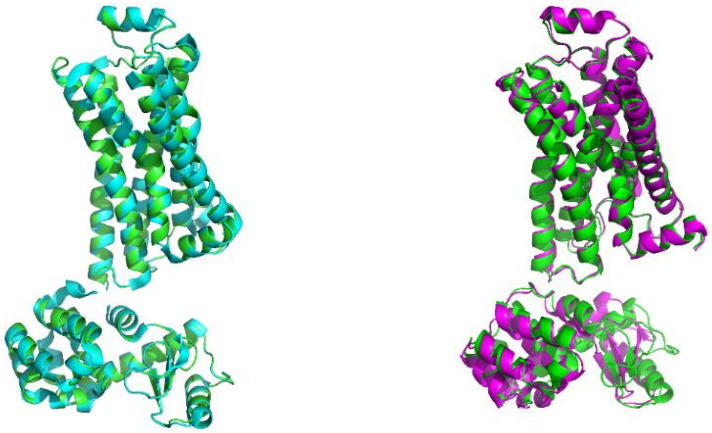

Figure 4.1 **Comparison of ß$_2$AR structures**. A. Superposition of MicroED structure(green) and XFEL structure(cyan) (PDB ID:6PS0) of ß2AR. B. Superposition of MicroED structure(green) and synchrotron structure(magenta) (PDB ID:2RH1) of ß2AR

4.3.2 Optimization of How to Locate Crystal

Data collection of MicroED data was one of the most tedious and time-consuming process of the MicroED study. The major challenge was localization of the protein crystals. Due to the limitation of the microscopy setting, UV screening of the EM grids was not accessible, thus, location of protein crystal was basically performed in a randomly manner, which was time consuming and low efficient. Based on the long period MicroED data collection experience, some principles were summarized. 1) Avoid ice crystal. Ice crystal was a major contamination or disturbance for the data collection which was formed inevitably during the grids plunging process. Ice crystals could be used to test the beam setting in the beginning of the data

collection; however, precious microscopy time would be wasted if researchers could not distinguish protein crystals from ice crystals. Ice crystals were usually hexagonal, and most of the ice crystals were isolate from the LCP residue. For the ice crystals embedded into LCP, size and shape were the factors to separate ice and protein crystals. Ice crystals were usually larger and with shaper boundaries. 2) Protein crystals were embedded into LCP residue. During the phase converting process, the lipid that used to form LCP dissociated and become small floating lipid droplets, however, the released protein crystals might still be embedded with LCP residual which enable them not to be removed by the filter paper during the EM grid preparation process. Therefore, most protein crystals on the grid were buried by LCP residual. 3) Protein crystals in the middle of mesh on the carbon film diffracted better. Although the carbon film on the EM grid was thin enough to not attenuate the contrast or resolution, it was noticed that the protein crystals located in the middle of the mesh diffracted better than the crystals that sit in the top of the carbon film completely, in both number of diffraction spots and resolution. The position of the protein crystals was uncontrollable, but it was always worth a shot for the crystals localized in the middle of the mesh.

4.4 Method

4.4.1 ß$_2$AR Expression, Purification, and Crystallization

This study utilized the previously described human ß$_2$AR construct with a Roth mutation (Ishchenko, 2019 #84)(Roth, 2008 #85). In brief, ß$_2$AR was expressed in *Spodoptera frugiperda* Sf9 insect cells with the baculovirus method (Expression

systems). Biomass was washed with low salt lysis buffer and high salt lysis buffer followed by solublization process which extract membrane protein with n-dodecyl-ß-D-maltoside (DDM, Anatrace). Extracted protein was purified with cobalt chelating sepharose chromatography. PNGase F was added to the purified ß2AR to remove the glycosylation modification. Deglycosylated ß2AR was concentrated to 40-50 mg/mL with a 100 kD concentrator (Sartorius) before crystallization.

The purified $ß_2$AR was reconstituted into LCP by mixing protein solution with melt lipid by syringe mixer (Hamilton) (Caffrey and Cherezov 2009). The LCP mixture consisted with 40% protein(v/v) and 60% lipid(v/v). The lipid was monoolein (Sigma) supplemented with 10 %(w/w) cholesterol (Anatrace). About 5 μL protein laden LCP was injected to another 100 μL air-tight syringe filling with about 60 μL precipitant solution (30-35% v/v PEG 400, 0.1-0.2 M Na_2SO4, 0.1 M Bis-tris propane pH 6.5-7.0, 5-7% 1,4-Butanediol) then the syringe was sealed and incubated at 20°C for 24 hours.

4.4.2 Phase Converting and Grids Preparation

The phase converting and grids preparation process was followed previously described protocol. In brief, $ß_2$AR crystallization was confirmed with microscope using cross polarized light. Then excess precipitant solution was removed from the syringe, multiple syringes could be combined to get sufficient sample during this step. Multiple additives including polyethylene glycol 400(PEG 400), 2-methyl-2,4-pentanediol (MPD), JeffimineM600 etc. could convert the viscous LCP to less viscous sponge like phase by direct mixing in the syringe (Zhu, Bu et al. 2020). Converting

ß2AR crystal embedded LCP by direct mixing with PEG 400 provided best result. Phase converted sample was deposited on the glow-discharged carbon EM grids (Quantifoil MultiA), then the grid was manually blotting for 12 seconds followed by vitrification with liquid ethane. Grids were stored in liquid nitrogen for future use.

4.4.3 Data collection and data processing

MicroED data of ß2AR was collected by Titan Krios with CETA CMOS collector. Plunged grids were loaded to the microscopy without any artificial modification such as cryo-fib to reduce the thickness of the crystals. Microscope was operated at 300 kV. The rotation speed of the stage was 0.12 °/s, and the exposer time of the detector was 5 seconds. Data sets of ß2AR were collected to cover about 30°.
MicroED data of ß2AR was converted from MRC format to smv format using the TVIPS tools software suite (Hattne, Reyes et al. 2015), which generated the images that could be processed by standard x-ray diffraction processing software. The MicroED data was indexed, integrated and scaled with XDSGUI (Kabsch 2010), diffraction data from three crystals was merged to build the model. Molecular replacement was employed to build the model with previously solved ß2AR LCP-SFX structure as the searching model. Both model building and refinement was processed by PHENIX (Afonine, Grosse-Kunstleve et al. 2012).

4.4.4 Data indexing and model refinement

73 diffraction datasets were collected from two vitrified grids, all of them are indexable but only 3 datasets were merged to build the model of β_2AR. Due to the orientation preference of the blade shaped crystals on the grids, the diffraction data of a cone that parallel to the incident electron beam was missing and could not be compensated by merging different dataset from different crystals. Merging too many datasets will jeopardize the statistics of the index result with very little increase of the completeness. A few diffraction patterns in the dataset showed clear diffraction spots at sub 3 Å region. The merged dataset result in an overall completeness of ~35 % at 3.97 Å resolution. The merged datasets were indexed in a space group $P2_12_12_1$(#19) with unit cell dimension a= 40.04 Å, b=74.44 Å, c=165.51 Å, α=90 °, β=90 °, γ=90 °. The unit cell parameters were consistent with the previous determined XFEL β_2AR structure which was used as the search model for the model building process of β_2AR MicroED structure. Due to the low completeness, the model of the β_2AR MicroED structure only showed electron density of the backbone. The seven transmembrane helixes were showed and fitted with the search model, most of the side chains were not seen in the density map. Compared to the XFEL structure determination of β_2AR, which merged diffraction pattern from 41416 crystal hits, structure determination of β_2AR with MicroED only need three or even less crystals. It indicates a significant advantage of MicroED method in which less crystals and smaller sized crystals are needed for structure determination.

Table 4.1. MicroED Crystallographic Table for β2AR

Data Processing	
Integration Wavelength (Å)	0.0197
Resolution range (Å)	25.89–3.95
Space group	P 21 21 21
Unit cell (a, b, c) (Å)	40.04, 74.44, 165.51
(α = β = γ) (°)	90, 90, 90
Completeness	34.3(%)
⟨I/σ(I)⟩	1.10
CC1/2	46.5
Refinement	
Rwork	0.2783 (0.3427)
Rfree	0.3479 (0.3664)
RMS (bonds) (Å)	0.003
RMS (angles) (°)	0.653
Ramachandran favored (%)	95.43
Ramachandran outliers (%)	0
Rotamer outliers (%)	0
Clashscore	6.10
Mean isotropic B factor	103.57

4.5 Discussion

4.5.1 Expand the Application Boundary

The proof of principal study has already showed the feasibility of MicroED to determine high resolution soluble protein structures. Recent years, MicroED has also been proved an efficient approach to study the small molecule structures. Compared to soluble protein crystal sample, small molecules were more ideal for MicroED because of the convenience for grid preparation and data collection. However, there is still a gap in MicroED application territory need to be filled, which is membrane protein structure determination. Our previous research has proved the LCP-MicroED method is applicable for determining atomic level protein structure from LCP embedded soluble protein crystals. This study expanded the application boundary of MicroED technology to membrane by solving the structure of a well-studied membrane protein target β_2AR. Although another GPCR, adenosine A_{2A} receptor(A_{2A}AR) was successfully solved recently by the combination of LCP-MicroED and cryo-FIB technology, our study does not require cryo-FIB to further pare the protein crystals on the grids, which enable more researchers who do not have the accessibility to cryo-FIB to apply LCP-MicroED technology.

4.5.2 Why Completeness Is Low

The completeness of ß2AR MicroED data was about 30%-40% which was relatively lower than the completeness needed for determine a high-resolution structure (Dauter, 1999 #111). The intrinsic reason of the low completeness was the thickness

of the crystal that electron beam needed to penetrate would increase while the sample stage rotating. The negatively charged electron beam can only penetrated couple hundred nanometers sample effectively, however, the thickness of β_2AR crystals was usually around micron level. The advantage of needle sized β_2AR crystals was the thickness of the tip region of the crystal was relatively thinner than the middle area, which enable the collection of good diffraction patterns. However, the needle shape crystals also had limitation. Because of the needle shape, when blotted the crystals on the EM grid, the orientation of crystals would not cover all the degrees in three-dimensions since it was impossible to blot a crystal that was perpendicular to the grids. Thus, during MicroED data collection, the rotation degree of the stage needs to be about 90° to ensure the coverage for all the orientations, which was limited by current cryo-EM setting (Nannenga, 2014). The theoretical space group of β_2AR crystal crystallized in the previously described condition was P 21 21 21, the poor symmetric nature of β_2AR crystal required nearly 180 ° coverage to reach the full completeness. In this perspective, β_2AR was a complicated target for MicroED study, nevertheless, we successfully collected high quality diffraction patterns as well as the rotationally collected movie. Therefore, protein crystals with better symmetry were expected to yield way higher completeness than β_2AR.

CHAPTER 5

CONCLUSIONS AND FUTURE PLANS

5.1 Histamine 4 Project

After 4 rounds construct optimization, compare with the wild type of histamine receptor, we successfully increased expression level and homogeneity of the target protein. However, binding with ligand didn't increase the thermostability of the protein which barely happen in GPCRs unless the GPCR was over engineered. Since the binding pocket was not modified directly, one possibility is the fusion protein B distorted the helix Ⅴ and helix Ⅵ , which change the conformation indirectly and prohibit the ligand binding.

The future plan could be divided in two directions. First direction is keep optimizing the junction site, fusion proteins, and mutations so that better construct could be generated. The second direction, fusion proteins could be fused on N-termini of histamine receptor. Since ICLⅢ was not touched, theoretically, histamine receptor could still interact with G protein. And the GPCR-G protein complex will make it possible to determine the structure using cryo-EM.

5.2 MicroED Project

During the rotational movie data collection process, the high-quality diffraction data did not last very long especially for the high-resolution region. Even the best dataset can only cover about 30-40 degrees, which is 1/3 of the maximum scope that the sample stage can tilt. The thickness of the crystal that electron beam needs to penetrate will increase when tilting the sample stage, which is one of the causes of low completeness. On the other hand, the increase of the sample thickness may theoretically increase the inelastic scattering effect, which may jeopardize the diffraction pattern collection. The interaction between electron and sample may lead to energy loss of the primary incident electron, which creates inelastic scattering. In conventional X-ray crystallography, the inelastic scattering was normally ignored since the energy level of x-ray beam was extremely high. However, inelastic scattering was unavoidable in electron diffraction which could be removed by energy filter. The electron microscope used to collect electron diffraction in this study has no energy filter installed, thus, diffraction pattern will get worse when the sample stage was tilted to a relatively high degree. It matched the fact that most of high-quality diffraction frames were collected from – 5 degrees to + 5 degrees. Energy filter eliminated the effect from electron that has different energy from the primary electron, which might increase the diffraction quality especially at the high tilting degree. Besides, to minimize the inelastic effect, the current setting of the electron microscope might employ relatively high electron dosage, which increase the radiation damage of the protein crystal sample. With the energy filter, the electron

dosage could be optimized to deliver high quality diffraction pattern and reduce the radiation damage, which ultimately increase the completeness of the data set.

To further prove this method, other suitable membrane protein targets could be studied. For GPCR, bacterial rhodopsin(bR) is a good candidate. According to previous bR study, the crystal packing of bR is symmetrical, therefor, when collecting rotational movie, small angle coverage could yield high completeness. The crystal shape of bR is plate like shape which is also preferred in MicroED study because of the natural low crystal thickness. Other membrane crystals with low thickness and high symmetry are suitable for MicroED method as well.

REFERENCES

Afonine, P. V., R. W. Grosse-Kunstleve, N. Echols, J. J. Headd, N. W. Moriarty, M. Mustyakimov, T. C. Terwilliger, A. Urzhumtsev, P. H. Zwart and P. D. Adams (2012). "Towards automated crystallographic structure refinement with phenix.refine." Acta Crystallogr D Biol Crystallogr **68**(Pt 4): 352-367.

Aherne, M., J. A. Lyons and M. Caffrey (2012). "A fast, simple and robust protocol for growing crystals in the lipidic cubic phase." J Appl Crystallogr **45**(Pt 6): 1330-1333.

Battye, T. G., L. Kontogiannis, O. Johnson, H. R. Powell and A. G. Leslie (2011). "iMOSFLM: a new graphical interface for diffraction-image processing with MOSFLM." Acta Crystallogr D Biol Crystallogr **67**(Pt 4): 271-281.

Batyuk, A., L. Galli, A. Ishchenko, G. W. Han, C. Gati, P. A. Popov, M. Y. Lee, B. Stauch, T. A. White, A. Barty, A. Aquila, M. S. Hunter, M. Liang, S. Boutet, M. Pu, Z. J. Liu, G. Nelson, D. James, C. Li, Y. Zhao, J. C. Spence, W. Liu, P. Fromme, V. Katritch, U. Weierstall, R. C. Stevens and V. Cherezov (2016). "Native phasing of x-ray free-electron laser data for a G protein-coupled receptor." Sci Adv **2**(9): e1600292.

Belrhali, H., P. Nollert, A. Royant, C. Menzel, J. P. Rosenbusch, E. M. Landau and E. Pebay-Peyroula (1999). "Protein, lipid and water organization in bacteriorhodopsin crystals: a molecular view of the purple membrane at 1.9 A resolution." Structure **7**(8): 909-917.

Bertram, N., T. Laursen, R. Barker, K. Bavishi, B. L. Moller and M. Cardenas (2015). "Nanodisc Films for Membrane Protein Studies by Neutron Reflection: Effect of the Protein Scaffold Choice." Langmuir **31**(30): 8386-8391.

Boutet, S. b., P. Fromme and M. S. Hunter (2018). X-ray Free Electron Lasers : A Revolution in Structural Biology. Cham, Springer International Publishing : Imprint: Springer,: 1 online resource (XVI, 479 pages 128 illustrations, 108 illustrations in color.

Briggs, J. and M. Caffrey (1994). "The temperature-composition phase diagram and mesophase structure characterization of monopentadecenoin in water." Biophys J **67**(4): 1594-1602.

Bu, G. and B. L. Nannenga (2021). "MicroED Sample Preparation and Data Collection For Protein Crystals." Methods Mol Biol **2215**: 287-297.

Caffrey, M. (2015). "A comprehensive review of the lipid cubic phase or in meso method for crystallizing membrane and soluble proteins and complexes." Acta Crystallogr F Struct Biol Commun **71**(Pt 1): 3-18.

Caffrey, M. and A. Cheng (1995). "Kinetics of lipid phase changes." Curr Opin Struct Biol **5**(4): 548-555.

Caffrey, M. and V. Cherezov (2009). "Crystallizing membrane proteins using lipidic mesophases." Nat Protoc **4**(5): 706-731.

Caffrey, M., D. Li and A. Dukkipati (2012). "Membrane protein structure determination using crystallography and lipidic mesophases: recent advances and successes." Biochemistry **51**(32): 6266-6288.

Caffrey, M., D. Li, N. Howe and S. T. Shah (2014). "'Hit and run' serial femtosecond crystallography of a membrane kinase in the lipid cubic phase." Philos Trans R Soc Lond B Biol Sci **369**(1647): 20130621.

Chayen, N. E. (1998). "Comparative studies of protein crystallization by vapour-diffusion and microbatch techniques." Acta Crystallogr D Biol Crystallogr **54**(Pt 1): 8-15.

Chen, V. B., W. B. Arendall, 3rd, J. J. Headd, D. A. Keedy, R. M. Immormino, G. J. Kapral, L. W. Murray, J. S. Richardson and D. C. Richardson (2010). "MolProbity: all-atom structure validation for macromolecular crystallography." Acta Crystallogr D Biol Crystallogr **66**(Pt 1): 12-21.

Cherezov, V. (2011). "Lipidic cubic phase technologies for membrane protein structural studies." Curr Opin Struct Biol **21**(4): 559-566.

Cherezov, V., J. Clogston, M. Z. Papiz and M. Caffrey (2006). "Room to move: crystallizing membrane proteins in swollen lipidic mesophases." J Mol Biol **357**(5): 1605-1618.

Cherezov, V., J. Liu, M. Griffith, M. A. Hanson and R. C. Stevens (2008). "LCP-FRAP Assay for Pre-Screening Membrane Proteins for in Meso Crystallization." Cryst Growth Des **8**(12): 4307-4315.

Cherezov, V., D. M. Rosenbaum, M. A. Hanson, S. G. Rasmussen, F. S. Thian, T. S. Kobilka, H. J. Choi, P. Kuhn, W. I. Weis, B. K. Kobilka and R. C. Stevens (2007). "High-resolution crystal structure of an engineered human beta2-adrenergic G protein-coupled receptor." Science **318**(5854): 1258-1265.

Chung, H. and M. Caffrey (1994). "The neutral area surface of the cubic mesophase: location and properties." Biophys J **66**(2 Pt 1): 377-381.

Congreve, M., C. Langmead and F. H. Marshall (2011). "The use of GPCR structures in drug design." Adv Pharmacol **62**: 1-36.

Congreve, M. and F. Marshall (2010). "The impact of GPCR structures on pharmacology and structure-based drug design." Br J Pharmacol **159**(5): 986-996.

Craven, B. M. (1976). "Crystal structure of cholesterol monohydrate." Nature **260**(5553): 727-729.

de la Cruz, M. J., J. Hattne, D. Shi, P. Seidler, J. Rodriguez, F. E. Reyes, M. R. Sawaya, D. Cascio, S. C. Weiss, S. K. Kim, C. S. Hinck, A. P. Hinck, G. Calero, D. Eisenberg and T. Gonen (2017). "Atomic-resolution structures from fragmented protein crystals with the cryoEM method MicroED." Nat Methods **14**(4): 399-402.

Dror, R. O., T. J. Mildorf, D. Hilger, A. Manglik, D. W. Borhani, D. H. Arlow, A. Philippsen, N. Villanueva, Z. Yang, M. T. Lerch, W. L. Hubbell, B. K. Kobilka, R. K. Sunahara and D. E. Shaw (2015). "SIGNAL TRANSDUCTION. Structural basis for nucleotide exchange in heterotrimeric G proteins." Science **348**(6241): 1361-1365.

Duyvesteyn, H. M. E., A. Kotecha, H. M. Ginn, C. W. Hecksel, E. V. Beale, F. de Haas, G. Evans, P. Zhang, W. Chiu and D. I. Stuart (2018). "Machining protein microcrystals for structure determination by electron diffraction." Proc Natl Acad Sci U S A **115**(38): 9569-9573.

El Ghachi, M., N. Howe, C. Y. Huang, V. Olieric, R. Warshamanage, T. Touze, D. Weichert, P. J. Stansfeld, M. Wang, F. Kerff and M. Caffrey (2018). "Crystal structure of undecaprenyl-pyrophosphate phosphatase and its role in peptidoglycan biosynthesis." Nat Commun **9**(1): 1078.

Emsley, P. and K. Cowtan (2004). "Coot: model-building tools for molecular graphics." Acta Crystallogr D Biol Crystallogr **60**(Pt 12 Pt 1): 2126-2132.

Emsley, P., B. Lohkamp, W. G. Scott and K. Cowtan (2010). "Features and development of Coot." Acta Crystallogr D Biol Crystallogr **66**(Pt 4): 486-501.

Evans, P. R. and G. N. Murshudov (2013). "How good are my data and what is the resolution?" Acta Crystallogr D Biol Crystallogr **69**(Pt 7): 1204-1214.

Faas, R., D. Kiefer, L. Job, A. Pohle, K. Moss, M. Henkel and R. Hausmann (2018). "Time-course and degradation rate of membrane scaffold protein (MSP1D1) during recombinant production." Biotechnol Rep (Amst) **17**: 45-48.

Faham, S. and J. U. Bowie (2002). "Bicelle crystallization: a new method for crystallizing membrane proteins yields a monomeric bacteriorhodopsin structure." J Mol Biol **316**(1): 1-6.

Gemmi, M., E. Mugnaioli, T. E. Gorelik, U. Kolb, L. Palatinus, P. Boullay, S. Hovmoller and J. P. Abrahams (2019). "3D Electron Diffraction: The Nanocrystallography Revolution." ACS Cent Sci **5**(8): 1315-1329.

Gruene, T., J. T. C. Wennmacher, C. Zaubitzer, J. J. Holstein, J. Heidler, A. Fecteau-Lefebvre, S. De Carlo, E. Muller, K. N. Goldie, I. Regeni, T. Li, G. Santiso-Quinones, G. Steinfeld, S. Handschin, E. van Genderen, J. A. van Bokhoven, G. H. Clever and R. Pantelic (2018). "Rapid Structure Determination of Microcrystalline Molecular Compounds Using Electron Diffraction." Angew Chem Int Ed Engl **57**(50): 16313-16317.

Gruss, F., S. Hiller and T. Maier (2015). "Purification and Bicelle Crystallization for Structure Determination of the E. coli Outer Membrane Protein TamA." Methods Mol Biol **1329**: 259-270.

Hanson, M. A., V. Cherezov, M. T. Griffith, C. B. Roth, V. P. Jaakola, E. Y. Chien, J. Velasquez, P. Kuhn and R. C. Stevens (2008). "A specific cholesterol binding site is established by the 2.8 A structure of the human beta2-adrenergic receptor." Structure **16**(6): 897-905.

Hattne, J., M. W. Martynowycz, P. A. Penczek and T. Gonen (2019). "MicroED with the Falcon III direct electron detector." IUCrJ **6**(Pt 5): 921-926.

Hattne, J., F. E. Reyes, B. L. Nannenga, D. Shi, M. J. de la Cruz, A. G. Leslie and T. Gonen (2015). "MicroED data collection and processing." Acta Crystallogr A Found Adv **71**(Pt 4): 353-360.

Hattne, J., D. Shi, M. J. de la Cruz, F. E. Reyes and T. Gonen (2016). "Modeling truncated pixel values of faint reflections in MicroED images." J Appl Crystallogr **49**(Pt 3): 1029-1034.

Hattne, J., D. Shi, C. Glynn, C. T. Zee, M. Gallagher-Jones, M. W. Martynowycz, J. A. Rodriguez and T. Gonen (2018). "Analysis of Global and Site-Specific Radiation Damage in Cryo-EM." Structure **26**(5): 759-766 e754.

Hilger, D., M. Masureel and B. K. Kobilka (2018). "Structure and dynamics of GPCR signaling complexes." Nat Struct Mol Biol **25**(1): 4-12.

Hu, G. M., T. L. Mai and C. M. Chen (2017). "Visualizing the GPCR Network: Classification and Evolution." Sci Rep **7**(1): 15495.

Huang, C. Y., V. Olieric, N. Howe, R. Warshamanage, T. Weinert, E. Panepucci, L. Vogeley, S. Basu, K. Diederichs, M. Caffrey and M. Wang (2018). "In situ serial crystallography for rapid de novo membrane protein structure determination." Commun Biol **1**: 124.

Huang, C. Y., V. Olieric, P. Ma, E. Panepucci, K. Diederichs, M. Wang and M. Caffrey (2015). "In meso in situ serial X-ray crystallography of soluble and membrane proteins." Acta Crystallogr D Biol Crystallogr **71**(Pt 6): 1238-1256.

Ishchenko, A., E. E. Abola and V. Cherezov (2017). "Crystallization of Membrane Proteins: An Overview." Methods Mol Biol **1607**: 117-141.

Ishchenko, A., L. Peng, E. Zinovev, A. Vlasov, S. C. Lee, A. Kuklin, A. Mishin, V. Borshchevskiy, Q. Zhang and V. Cherezov (2017). "Chemically Stable Lipids for Membrane Protein Crystallization." Cryst Growth Des **17**(6): 3502-3511.

Jaeger, K., S. Bruenle, T. Weinert, W. Guba, J. Muehle, T. Miyazaki, M. Weber, A. Furrer, N. Haenggi, T. Tetaz, C. Y. Huang, D. Mattle, J. M. Vonach, A. Gast, A. Kuglstatter, M. G. Rudolph, P. Nogly, J. Benz, R. J. P. Dawson and J. Standfuss (2019). "Structural Basis for Allosteric Ligand Recognition in the Human CC Chemokine Receptor 7." Cell **178**(5): 1222-1230 e1210.

Johansson, L. C., B. Stauch, A. Ishchenko and V. Cherezov (2017). "A Bright Future for Serial Femtosecond Crystallography with XFELs." Trends Biochem Sci **42**(9): 749-762.

Jones, C. G., M. W. Martynowycz, J. Hattne, T. J. Fulton, B. M. Stoltz, J. A. Rodriguez, H. M. Nelson and T. Gonen (2018). "The CryoEM Method MicroED as a Powerful Tool for Small Molecule Structure Determination." ACS Cent Sci **4**(11): 1587-1592.

Kabsch, W. (2010). "Xds." Acta Crystallogr D Biol Crystallogr **66**(Pt 2): 125-132.

Katritch, V., V. Cherezov and R. C. Stevens (2013). "Structure-function of the G protein-coupled receptor superfamily." Annu Rev Pharmacol Toxicol **53**: 531-556.

Kijac, A. Z., Y. Li, S. G. Sligar and C. M. Rienstra (2007). "Magic-angle spinning solid-state NMR spectroscopy of nanodisc-embedded human CYP3A4." Biochemistry **46**(48): 13696-13703.

Koehl, A., H. Hu, S. Maeda, Y. Zhang, Q. Qu, J. M. Paggi, N. R. Latorraca, D. Hilger, R. Dawson, H. Matile, G. F. X. Schertler, S. Granier, W. I. Weis, R. O. Dror, A. Manglik, G. Skiniotis and B. K. Kobilka (2018). "Structure of the micro-opioid receptor-Gi protein complex." Nature **558**(7711): 547-552.

Kremer, J. R., D. N. Mastronarde and J. R. McIntosh (1996). "Computer visualization of three-dimensional image data using IMOD." J Struct Biol **116**(1): 71-76.

Lan, Z., M. Y. Lee, E. Chun, B. Liu and W. Liu (2019). "Overview of Biochemical Assays in Lipidic Cubic Phase." Trends Biochem Sci **44**(4): 295-299.

Landau, E. M. and J. P. Rosenbusch (1996). "Lipidic cubic phases: a novel concept for the crystallization of membrane proteins." Proc Natl Acad Sci U S A **93**(25): 14532-14535.

Levine, A. M., G. Bu, S. Biswas, E. H. R. Tsai, A. B. Braunschweig and B. L. Nannenga (2020). "Crystal structure and orientation of organic semiconductor thin films by microcrystal electron diffraction and grazing-incidence wide-angle X-ray scattering." Chem Commun (Camb) **56**(30): 4204-4207.

Li, D. and M. Caffrey (2011). "Lipid cubic phase as a membrane mimetic for integral membrane protein enzymes." Proc Natl Acad Sci U S A **108**(21): 8639-8644.

Li, D., N. Howe, A. Dukkipati, S. T. Shah, B. D. Bax, C. Edge, A. Bridges, P. Hardwicke, O. M. Singh, G. Giblin, A. Pautsch, R. Pfau, G. Schnapp, M. Wang, V. Olieric and M. Caffrey (2014). "Crystallizing Membrane Proteins in the Lipidic Mesophase. Experience with Human Prostaglandin E2 Synthase 1 and an Evolving Strategy." Cryst Growth Des **14**(4): 2034-2047.

Li, D., P. J. Stansfeld, M. S. P. Sansom, A. Keogh, L. Vogeley, N. Howe, J. A. Lyons, D. Aragao, P. Fromme, R. Fromme, S. Basu, I. Grotjohann, C. Kupitz, K. Rendek, U. Weierstall, N. A. Zatsepin, V. Cherezov, W. Liu, S. Bandaru, N. J. English, C. Gati, A. Barty, O. Yefanov, H. N. Chapman, K. Diederichs, M. Messerschmidt, S. Boutet, G. J. Williams, M. Marvin Seibert and M. Caffrey (2015). "Ternary structure reveals mechanism of a membrane diacylglycerol kinase." Nat Commun **6**: 10140.

Liu, W. and V. Cherezov (2011). "Crystallization of membrane proteins in lipidic mesophases." J Vis Exp(49).

Liu, W., E. Chun, A. A. Thompson, P. Chubukov, F. Xu, V. Katritch, G. W. Han, C. B. Roth, L. H. Heitman, I. J. AP, V. Cherezov and R. C. Stevens (2012). "Structural basis for allosteric regulation of GPCRs by sodium ions." Science **337**(6091): 232-236.

Liu, W., M. A. Hanson, R. C. Stevens and V. Cherezov (2010). "LCP-Tm: an assay to measure and understand stability of membrane proteins in a membrane environment." Biophys J **98**(8): 1539-1548.

Liu, W., A. Ishchenko and V. Cherezov (2014). "Preparation of microcrystals in lipidic cubic phase for serial femtosecond crystallography." Nat Protoc **9**(9): 2123-2134.

Liu, W., D. Wacker, C. Gati, G. W. Han, D. James, D. Wang, G. Nelson, U. Weierstall, V. Katritch, A. Barty, N. A. Zatsepin, D. Li, M. Messerschmidt, S. Boutet, G. J. Williams, J. E. Koglin, M. M. Seibert, C. Wang, S. T. Shah, S. Basu, R. Fromme, C. Kupitz, K. N. Rendek, I. Grotjohann, P. Fromme, R. A. Kirian, K. R. Beyerlein, T. A. White, H. N. Chapman, M. Caffrey, J. C. Spence, R. C. Stevens and V. Cherezov (2013). "Serial femtosecond crystallography of G protein-coupled receptors." Science **342**(6165): 1521-1524.

Ma, P., D. Weichert, L. A. Aleksandrov, T. J. Jensen, J. R. Riordan, X. Liu, B. K. Kobilka and M. Caffrey (2017). "The cubicon method for concentrating membrane proteins in the cubic mesophase." Nat Protoc **12**(9): 1745-1762.

Martin-Garcia, J. M., C. E. Conrad, G. Nelson, N. Stander, N. A. Zatsepin, J. Zook, L. Zhu, J. Geiger, E. Chun, D. Kissick, M. C. Hilgart, C. Ogata, A. Ishchenko, N. Nagaratnam, S. Roy-Chowdhury, J. Coe, G. Subramanian, A. Schaffer, D. James, G. Ketwala, N. Venugopalan, S. Xu, S. Corcoran, D. Ferguson, U. Weierstall, J. C. H. Spence, V. Cherezov, P. Fromme, R. F. Fischetti and W. Liu (2017). "Serial millisecond crystallography of membrane and soluble protein microcrystals using synchrotron radiation." IUCrJ **4**(Pt 4): 439-454.

Martin-Garcia, J. M., L. Zhu, D. Mendez, M. Y. Lee, E. Chun, C. Li, H. Hu, G. Subramanian, D. Kissick, C. Ogata, R. Henning, A. Ishchenko, Z. Dobson, S. Zhang, U. Weierstall, J. C. H. Spence, P. Fromme, N. A. Zatsepin, R. F. Fischetti, V. Cherezov and W. Liu (2019). "High-viscosity injector-based pink-beam serial crystallography of microcrystals at a synchrotron radiation source." IUCrJ **6**(Pt 3): 412-425.

Martynowycz, M. W., W. Zhao, J. Hattne, G. J. Jensen and T. Gonen (2019). "Collection of Continuous Rotation MicroED Data from Ion Beam-Milled Crystals of Any Size." Structure **27**(3): 545-548 e542.

Martynowycz, M. W., W. Zhao, J. Hattne, G. J. Jensen and T. Gonen (2019). "Qualitative Analyses of Polishing and Precoating FIB Milled Crystals for MicroED." Structure **27**(10): 1594-1600 e1592.

Mastronarde, D. N. (2008). "Correction for non-perpendicularity of beam and tilt axis in tomographic reconstructions with the IMOD package." J Microsc **230**(Pt 2): 212-217.

McCoy, A. J., R. W. Grosse-Kunstleve, P. D. Adams, M. D. Winn, L. C. Storoni and R. J. Read (2007). "Phaser crystallographic software." J Appl Crystallogr **40**(Pt 4): 658-674.

Michel, S., J. Huet and F. Laval (1983). "Interactions between 9-hydroxyellipticine and X rays on mammalian cell survival in vitro." Radiat Res **96**(3): 592-602.

Mu, X., C. Gillman, C. Nguyen and T. Gonen (2021). "An Overview of Microcrystal Electron Diffraction (MicroED)." Annu Rev Biochem **90**: 431-450.

Nannenga, B. L. and T. Gonen (2016). "MicroED opens a new era for biological structure determination." Curr Opin Struct Biol **40**: 128-135.

Nannenga, B. L. and T. Gonen (2018). "MicroED: a versatile cryoEM method for structure determination." Emerg Top Life Sci **2**(1): 1-8.

Nannenga, B. L. and T. Gonen (2019). "The cryo-EM method microcrystal electron diffraction (MicroED)." Nat Methods **16**(5): 369-379.

Nannenga, B. L., D. Shi, J. Hattne, F. E. Reyes and T. Gonen (2014). "Structure of catalase determined by MicroED." Elife **3**: e03600.

Nannenga, B. L., D. Shi, A. G. W. Leslie and T. Gonen (2014). "High-resolution structure determination by continuous-rotation data collection in MicroED." Nat Methods **11**(9): 927-930.

Nogly, P., T. Weinert, D. James, S. Carbajo, D. Ozerov, A. Furrer, D. Gashi, V. Borin, P. Skopintsev, K. Jaeger, K. Nass, P. Bath, R. Bosman, J. Koglin, M. Seaberg, T. Lane, D. Kekilli, S. Brunle, T. Tanaka, W. Wu, C. Milne, T. White, A. Barty, U. Weierstall, V. Panneels, E. Nango, S. Iwata, M. Hunter, I. Schapiro, G. Schertler, R. Neutze and J. Standfuss (2018). "Retinal isomerization in bacteriorhodopsin captured by a femtosecond x-ray laser." Science **361**(6398).

Nollert, P. and E. M. Landau (1998). "Enzymic release of crystals from lipidic cubic phases." Biochem Soc Trans **26**(4): 709-713.

Nollert, P., J. Navarro and E. M. Landau (2002). "Crystallization of membrane proteins in cubo." Methods Enzymol **343**: 183-199.

Ohmer, C. J., M. Dasgupta, A. Patwardhan, I. Bogacz, C. Kaminsky, M. D. Doyle, P. Y. Chen, S. M. Keable, H. Makita, P. S. Simon, R. Massad, T. Fransson, R. Chatterjee, A. Bhowmick, D. W. Paley, N. W. Moriarty, A. S. Brewster, L. B. Gee, R. Alonso-Mori, F. Moss, F. D. Fuller, A. Batyuk, N. K. Sauter, U. Bergmann, C. L. Drennan, V. K. Yachandra, J. Yano, J. F. Kern and S. W. Ragsdale (2022). "XFEL serial crystallography reveals the room temperature structure of methyl-coenzyme M reductase." J Inorg Biochem **230**: 111768.

Panneels, V., W. Wu, C. J. Tsai, P. Nogly, J. Rheinberger, K. Jaeger, G. Cicchetti, C. Gati, L. M. Kick, L. Sala, G. Capitani, C. Milne, C. Padeste, B. Pedrini, X. D. Li, J. Standfuss, R. Abela and G. Schertler (2015). "Time-resolved structural studies with serial crystallography: A new light on retinal proteins." Struct Dyn **2**(4): 041718.

Pebay-Peyroula, E., G. Rummel, J. P. Rosenbusch and E. M. Landau (1997). "X-ray structure of bacteriorhodopsin at 2.5 angstroms from microcrystals grown in lipidic cubic phases." Science **277**(5332): 1676-1681.

Poulos, S., J. L. Morgan, J. Zimmer and S. Faham (2015). "Bicelles coming of age: an empirical approach to bicelle crystallization." Methods Enzymol **557**: 393-416.

Qiu, H. and M. Caffrey (2000). "The phase diagram of the monoolein/water system: metastability and equilibrium aspects." Biomaterials **21**(3): 223-234.

Robertson, J. L. (2018). "The lipid bilayer membrane and its protein constituents." J Gen Physiol **150**(11): 1472-1483.

Shi, D., B. L. Nannenga, M. J. de la Cruz, J. Liu, S. Sawtelle, G. Calero, F. E. Reyes, J. Hattne and T. Gonen (2016). "The collection of MicroED data for macromolecular crystallography." Nat Protoc **11**(5): 895-904.

Shi, D., B. L. Nannenga, M. G. Iadanza and T. Gonen (2013). "Three-dimensional electron crystallography of protein microcrystals." Elife **2**: e01345.

Shi, Y. (2014). "A glimpse of structural biology through X-ray crystallography." Cell **159**(5): 995-1014.

Shimamura, T., M. Shiroishi, S. Weyand, H. Tsujimoto, G. Winter, V. Katritch, R. Abagyan, V. Cherezov, W. Liu, G. W. Han, T. Kobayashi, R. C. Stevens and S. Iwata (2011). "Structure of the human histamine H1 receptor complex with doxepin." Nature **475**(7354): 65-70.

Soubias, O. and K. Gawrisch (2012). "The role of the lipid matrix for structure and function of the GPCR rhodopsin." Biochim Biophys Acta **1818**(2): 234-240.

Stauch, B. and V. Cherezov (2018). "Serial Femtosecond Crystallography of G Protein-Coupled Receptors." Annu Rev Biophys **47**: 377-397.

Thangam, E. B., E. A. Jemima, H. Singh, M. S. Baig, M. Khan, C. B. Mathias, M. K. Church and R. Saluja (2018). "The Role of Histamine and Histamine Receptors in Mast Cell-Mediated Allergy and Inflammation: The Hunt for New Therapeutic Targets." Front Immunol **9**: 1873.

Varsano, N., F. Beghi, N. Elad, E. Pereiro, T. Dadosh, I. Pinkas, A. J. Perez-Berna, X. Jin, H. S. Kruth, L. Leiserowitz and L. Addadi (2018). "Two polymorphic cholesterol monohydrate crystal structures form in macrophage culture models of atherosclerosis." Proc Natl Acad Sci U S A **115**(30): 7662-7669.

Velankar, S., S. K. Burley, G. Kurisu, J. C. Hoch and J. L. Markley (2021). "The Protein Data Bank Archive." Methods Mol Biol **2305**: 3-21.

Vergara, S., D. A. Lukes, M. W. Martynowycz, U. Santiago, G. Plascencia-Villa, S. C. Weiss, M. J. de la Cruz, D. M. Black, M. M. Alvarez, X. Lopez-Lozano, C. O. Barnes, G. Lin, H. C. Weissker, R. L. Whetten, T. Gonen, M. J. Yacaman and G. Calero (2017). "MicroED Structure of Au146(p-MBA)57 at Subatomic Resolution Reveals a Twinned FCC Cluster." J Phys Chem Lett **8**(22): 5523-5530.

Vogeley, L., T. El Arnaout, J. Bailey, P. J. Stansfeld, C. Boland and M. Caffrey (2016). "Structural basis of lipoprotein signal peptidase II action and inhibition by the antibiotic globomycin." Science **351**(6275): 876-880.

Wadsten, P., A. B. Wohri, A. Snijder, G. Katona, A. T. Gardiner, R. J. Cogdell, R. Neutze and S. Engstrom (2006). "Lipidic sponge phase crystallization of membrane proteins." J Mol Biol **364**(1): 44-53.

Weierstall, U., D. James, C. Wang, T. A. White, D. Wang, W. Liu, J. C. Spence, R. Bruce Doak, G. Nelson, P. Fromme, R. Fromme, I. Grotjohann, C. Kupitz, N. A. Zatsepin, H. Liu, S. Basu, D. Wacker, G. W. Han, V. Katritch, S. Boutet, M. Messerschmidt, G. J. Williams, J. E. Koglin, M. Marvin Seibert, M. Klinker, C. Gati, R. L. Shoeman, A. Barty, H. N. Chapman, R. A. Kirian, K. R. Beyerlein, R. C. Stevens, D. Li, S. T. Shah, N. Howe, M. Caffrey and V. Cherezov (2014). "Lipidic cubic phase injector facilitates membrane protein serial femtosecond crystallography." Nat Commun **5**: 3309.

Weinert, T., N. Olieric, R. Cheng, S. Brunle, D. James, D. Ozerov, D. Gashi, L. Vera, M. Marsh, K. Jaeger, F. Dworkowski, E. Panepucci, S. Basu, P. Skopintsev, A. S. Dore, T. Geng, R. M. Cooke, M. Liang, A. E. Prota, V. Panneels, P. Nogly, U. Ermler, G. Schertler, M. Hennig, M. O. Steinmetz, M. Wang and J. Standfuss (2017). "Serial millisecond crystallography for routine room-temperature structure determination at synchrotrons." Nat Commun **8**(1): 542.

Weinert, T., P. Skopintsev, D. James, F. Dworkowski, E. Panepucci, D. Kekilli, A. Furrer, S. Brunle, S. Mous, D. Ozerov, P. Nogly, M. Wang and J. Standfuss (2019). "Proton uptake mechanism in bacteriorhodopsin captured by serial synchrotron crystallography." Science **365**(6448): 61-65.

Winkler, M. B. L., R. T. Kidmose, M. Szomek, K. Thaysen, S. Rawson, S. P. Muench, D. Wustner and B. P. Pedersen (2019). "Structural Insight into Eukaryotic Sterol Transport through Niemann-Pick Type C Proteins." Cell **179**(2): 485-497 e418.

Xiang, J., E. Chun, C. Liu, L. Jing, Z. Al-Sahouri, L. Zhu and W. Liu (2016). "Successful Strategies to Determine High-Resolution Structures of GPCRs." Trends Pharmacol Sci **37**(12): 1055-1069.

Yonekura, K., K. Kato, M. Ogasawara, M. Tomita and C. Toyoshima (2015). "Electron crystallography of ultrathin 3D protein crystals: atomic model with charges." Proc Natl Acad Sci U S A **112**(11): 3368-3373.

Zabara, A., J. T. Y. Chong, I. Martiel, L. Stark, B. A. Cromer, C. Speziale, C. J. Drummond and R. Mezzenga (2018). "Design of ultra-swollen lipidic mesophases for the crystallization of membrane proteins with large extracellular domains." Nat Commun **9**(1): 544.

Zhu, L., G. Bu, L. Jing, D. Shi, M. Y. Lee, T. Gonen, W. Liu and B. L. Nannenga (2020). "Structure Determination from Lipidic Cubic Phase Embedded Microcrystals by MicroED." Structure **28**(10): 1149-1159 e1144.

APPENDIX A

PERMISSION OF FIGURE 1

ELSEVIER LICENSE
TERMS AND CONDITIONS

Apr 13, 2022

This Agreement between Liang Jing ("You") and Elsevier ("Elsevier") consists of your license details and the terms and conditions provided by Elsevier and Copyright Clearance Center.

License Number	5287290086174
License date	Apr 13, 2022
Licensed Content Publisher	Elsevier
Licensed Content Publication	Structure
Licensed Content Title	Status of GPCR Modeling and Docking as Reflected by Community-wide GPCR Dock 2010 Assessment
Licensed Content Author	Irina Kufareva,Manuel Rueda,Vsevolod Katritch,Raymond C. Stevens,Ruben Abagyan
Licensed Content Date	Aug 10, 2011
Licensed Content Volume	19
Licensed Content Issue	8
Licensed Content Pages	19
Start Page	1108

End Page	1126
Type of Use	reuse in a thesis/dissertation
Portion	figures/tables/illustrations
Number of figures/tables/illustrations	1
Format	both print and electronic
Are you the author of this Elsevier article?	No
Will you be translating?	No
Title	Research Assistant
Institution name	Arizona State University
Expected presentation date	May 2022
Portions	Figure 9 GPCR Phylogenetic Tree Highlighting the Recently Solved GPCR Structures and Their Homologs
Requestor Location	Liang Jing 1718 S longmore 68 MESA, AZ 85202 United States Attn: Liang Jing
Publisher Tax ID	98-0397604

APPENDIX B

PERMISSION OF FIGURE 6

ELSEVIER LICENSE
TERMS AND CONDITIONS

Apr 13, 2022

This Agreement between Liang Jing ("You") and Elsevier ("Elsevier") consists of your license details and the terms and conditions provided by Elsevier and Copyright Clearance Center.

License Number	5287310538279
License date	Apr 13, 2022
Licensed Content Publisher	Elsevier
Licensed Content Publication	Current Opinion in Structural Biology
Licensed Content Title	Protein structure determination by MicroED
Licensed Content Author	Brent L Nannenga,Tamir Gonen
Licensed Content Date	Aug 1, 2014
Licensed Content Volume	27
Licensed Content Issue	n/a
Licensed Content Pages	8
Start Page	24
End Page	31
Type of Use	reuse in a thesis/dissertation

Portion	figures/tables/illustrations
Number of figures/tables/illustrations	1
Format	both print and electronic
Are you the author of this Elsevier article?	No
Will you be translating?	No
Title	Research Assistant
Institution name	Arizona State University
Expected presentation date	May 2022
Portions	Figure 2. MicroED data collection and microcrystal visualization
Requestor Location	Liang Jing 1718 S longmore 68 MESA, AZ 85202 United States Attn: Liang Jing
Publisher Tax ID	98-0397604